SNX10 regulates the clearance of mitochondrial proteins and mitochondrial bioenergetics

Laura Trachsel-Moncho[1,2,3], Benan John Mathai[1,2,3#], Chiara Veroni[1,2,3#], Ana Lapao[1,2], Sakshi Singh[1,2], Nagham Theres Asp[1,2], Sebastian W. Schultz [2,3], Serhiy Pankiv[1,2], Anne Simonsen[1,2,3;*]

[1] Department of Molecular Medicine, Institute of Basic Medical Sciences Faculty of Medicine, University of Oslo, 1112 Blindern, Oslo 0317, Norway

[2] Centre for Cancer Cell Reprogramming, Institute of Clinical Medicine, Faculty of Medicine, University of Oslo, Oslo, Norway

[3] Department of Molecular Cell Biology, Institute for Cancer Research, Oslo University Hospital, Montebello, 0379 Oslo, Norway

[#] These authors contributed equally

*Corresponding author. E-mail; anne.simonsen@medisin.uio.no

Keywords: mitophagy, autophagy, SNX10, endosomes, endocytosis, mitochondria, mitochondrial homeostasis

Short title: SNX10 regulates mitochondrial homeostasis

Summary:

Trachsel-Moncho et al. identify the endosomal protein SNX10 as a regulator of mitochondrial homeostasis. They show that SNX10 vesicles contain selected mitochondrial proteins and that depletion of SNX10 impairs mitochondrial respiration in cells and increases reactive oxygen species levels and cell death in vivo.

ABSTRACT

We here show that SNX10 localizes to endocytic compartments in a PtdIns3P-dependent manner and that mutations in the PX domain associated with autosomal recessive osteopetrosis prevent its endosomal recruitment. We demonstrate that SNX10 regulates endosomal trafficking but also interacts with mitochondrial proteins and shows dynamic interactions with mitochondria. Intriguingly, SNX10 and RAB5A-positive vesicles contain mitochondrial material and stain positive for LC3B. SNX10-positive vesicles contain COX-IV and SAMM50, both proteins being important for mitochondrial respiratory chain function, while other mitochondrial proteins are excluded. We find that depletion of SNX10 results in lower levels of COX-IV and SAMM50 both in vitro and in a zebrafish model, as well as impaired mitochondrial respiration and reduced citrate synthase activity, indicating a role for SNX10 as a regulator of mitochondrial bioenergetics. Importantly, the knockout of SNX10 homologs in zebrafish led to elevated ROS levels and cell death, demonstrating the in vivo relevance of SNX10-mediated regulation of mitochondrial homeostasis.

INTRODUTION

Several diseases are characterized by an imbalance between protein production, sorting and degradation, making it important to understand the crosstalk between the pathways involved in regulation of proteostasis, including autophagy and endocytosis[1]. While macroautophagy (hereafter autophagy) entails the sequestration of endogenous cytoplasmic material into double-membrane autophagosomes that fuse with lysosomes for cargo degradation[2,3], endocytosis generally involves lysosomal sorting of exogenous material. The autophagic and endocytic pathways are however closely connected, as autophagosomes can fuse with endocytic vesicles prior to their fusion with lysosomes and endosomes can contribute membrane to the growing autophagosome[4]. Moreover, components of the core autophagy machinery have been localized to endosomes, and components of the endosomal sorting complexes required for transport (ESCRT) are important for closure of the autophagosome[5]. However, our knowledge about the molecular mechanisms involved in the regulation of the dynamic crosstalk between different types of autophagy and endocytosis remains sparse.

Mitophagy involves the selective degradation of damaged mitochondria in lysosomes, preventing their accumulation and mitigating cellular stress. Dysregulation of mitophagy is linked to neurodegenerative diseases, metabolic disorders, and cancer and it is therefore important to understand the mechanisms involved in mitophagy. Recently, it has been observed that early and late endosomes can interact with mitochondria[6–10] and that such interactions may play a role in mitochondrial quality control and stress responses[11].

The PX domain-containing protein sorting nexin 10 (SNX10) was recently identified as a putative regulator of mitophagy in a screen for lipid-binding proteins involved in the regulation of Parkin-independent mitophagy[12]. SNX10 is one of the simplest of the SNX (Sorting nexin) family proteins, consisting of a single PX domain that interacts with PtdIns(3)P[13] and an intrinsically disordered region (IDR) in its C-terminal domain, as elucidated by AlphaFold[14,15]. The IDR may account for the diverse cellular roles attributed to SNX10 and its implication in various pathologies[16]. SNX10 has been found to play a role in cilium biogenesis and promote the localization of vacuolar H^+-ATPase subunits and RAB8A to the cilium[17]. Moreover, several single nucleotide polymorphisms (SNPs) in SNX10 have been linked to autosomal recessive osteopetrosis (ARO)[18–21], a rare and heterogeneous genetic disease characterized by abnormally dense bone, where dysfunctional or absent osteoclasts fail at performing bone resorption[18]. SNX10 mutations are linked to approximately 4% of the reported ARO cases[18,19]. Beyond ARO, SNX10 has emerged as a

multifaceted player in various pathologies, including gastric cancer, glioblastoma, and colorectal cancer[22–24]. Moreover, SNX10 deficiency has been reported to reshape macrophage polarization towards an anti-inflammatory M2 phenotype[25], while its upregulation during bacterial infection enhances phagosome maturation and bacterial killing[26]. Additionally, SNX10 expression seems to correlate with the severity of Crohn's Disease in both human and mouse models, suggesting its potential role in inflammatory bowel diseases[27]. SNX10 has also been found to influence human adipocyte differentiation and function[28]. The involvement of SNX10 in diverse diseases, necessities a deeper exploration of its molecular mechanisms and therapeutic potential.

Here we show that SNX10 localizes to early and late endocytic compartments and that it functions as a negative regulator of mitochondrial abundance and bioenergetics.

Results

SNX10 localizes to early and late endocytic compartments in a PtdIns3P dependent manner

To characterize the mechanisms underlying the normal function of SNX10 and its role in disease development, we generated U2OS cell lines with stable inducible expression of EGFP-tagged wild type (WT) SNX10 or SNX10 having mutations corresponding to ARO-linked SNPs (Y32S, R51P or R51Q), all located in the PX domain[29] of the canonical SNX10 isoform (which contains a full length PX domain unlike the shorter isoform which lacks the first 84 amino acids) (Fig. 1A and Supplementary Fig. 1A and B). We observed small cytosolic puncta and larger ring shaped SNX10-positive structures in cells expressing WT SNX10-EGFP that were absent in cells expressing the ARO-linked mutants, all showing a diffuse cytosolic localization (Fig. 1B). The ARO mutants also seem more unstable, as several degradation products, not present in the WT cell lysate, were detected (Fig. 1C).

The small SNX10-EGFP positive puncta colocalized extensively with early endosome antigen 1 (EEA1) and were often seen in very close proximity to larger SNX10-positive ring structures, suggesting these might fuse (Fig. 1D). While SNX10 stained the whole limiting membrane, EEA1 was detected in membrane micro-domains on the larger ring structures (Fig. 1D). The diffuse cytosolic staining of the SNX10 mutants (Fig. 1B and D) indicates that the membrane localization of SNX10 is PtdIns3P dependent. Indeed, when treating cells with the PIK3C3 specific inhibitor VPS34-IN1, both the SNX10-EGFP positive puncta and the ring structures disappeared (Fig. 1D), as well as most of the EEA1 staining, as expected since EEA1 has a PtdIns3P-binding FYVE domain[30] (Fig. 1D).

In line with previous findings[31], we found that expression of SNX10-EGFP led to the formation of giant juxtanuclear vacuoles (Fig. 1B). Remarkably, these big vacuoles were negative for SNX10-EGFP and did not form in cells expressing mutant SNX10-EGFP (Y32S, R51P or R51Q) (Fig. 1A-B). Intriguingly, the limiting membrane of the large SNX10-induced vacuoles stained positive for LAMP1 (Fig. 1E), and the vacuole lumen stained with LysoTracker Red (Supplementary Fig. 1C), indicating an acidic lysosomal nature of the large SNX10-induced vacuoles. The medium to large SNX10 positive structures also presented an accumulation of LysoTracker Red (Supplementary Fig. 1C).

To further investigate the subcellular localization of SNX10 within the endocytic pathway, SNX10-EGFP cells were transduced with lentivirus encoding various mScarlet-tagged RAB proteins. In line with its localization to EEA1-positive endosomes (Fig. 1D), SNX10-EGFP colocalized with mScarlet-RAB5 (Fig. 1F), confirming its presence on early endosomes. However, SNX10- EGFP did not colocalize with mScarlet-RAB4 or mScarlet-RAB11, indicating that SNX10 is absent from recycling endosomes (Supplementary Fig. 1D). A partial colocalization with mScarlet-RAB7A (a marker of early-to-late endosomes) and mScarlet-RAB9A (involved in endosome-trans Golgi network trafficking) was observed (Fig. 1F), while no colocalization was detected with mScarlet-RAB6 (associated with secretion) or mScarlet-RAB43 (involved in retrograde transport) (Supplementary Fig. 1D). Both mScarlet-RAB7 and mScarlet-RAB9 also localized to the large vacuoles formed in cells overexpressing SNX10-EGFP, corroborating their late endosomal nature.

To further characterize the nature of SNX10 positive vesicles, SNX10-EGFP cells were processed for correlative light and electron microscopy (CLEM) analysis (Fig. 1G i-ii). When focusing in on one of the SNX10-EGFP positive structures, we could see endocytic vesicles containing membranous material (Fig. 1G iii-iv) that were surrounded by an electron-dense environment of small vesicles, where many appeared to be clathrin-coated vesicles (Fig. 1G iv, arrows). Indeed, using confocal imaging we could confirm that SNX10-EGFP localizes with clathrin-positive structures (Supplementary Fig. 1E).

SNX10 regulates the endocytic pathway

The localization of SNX10 to both early and late endocytic compartments led us to investigate a potential role of SNX10 in endosomal trafficking. U2OS SNX10-EGFP cells were incubated with an antibody against the epidermal growth factor (EGF) receptor (EGFR) on ice, followed by EGF-mediated stimulation of EGFR internalization (Fig. 2A). As expected, SNX10-EGFP puncta showed

a clear co-occurrence with endocytosed EGF and with EGFR after EGF stimulation (Fig. 2B). To address whether depletion of SNX10 would affect EGFR trafficking and/or signaling, SNX10 was depleted for 72 h, followed by incubation with EGF for 15 min to activate EGFR signaling and internalization. Intriguingly, both the total level of EGFR and the level of phosphorylated EGFR were increased in SNX10 depleted cells compared to control cells (Fig. 2C-D). As EGFR becomes de-phosphorylated upon its internalization into multi-vesicular bodies (MVBs), our data indicate a role for SNX10 as a regulator of endosome maturation and EGFR endosomal trafficking. In line with such a model, we found that SNX10 silencing with two independent oligos (Supplementary Fig. 2A) increased the numbers of EEA1-positive puncta (Fig. 2E-F). Moreover, quantification of endosomes containing immunogold-labelled EGFR in sections from electron microscopy images revealed that EGFR-containing endosomes were smaller in SNX10 depleted cells (Fig. 2G-H). Together, our data indicate a role for SNX10 in endosomal maturation, affecting the trafficking of EGFR.

SNX10-positive endosomes interact with mitochondria and contain mitochondrial material

To further understand the cellular function of SNX10, we set out to identify the interactome of SNX10 and compared it to the interactome of the mutant SNX10 Y32S that does not bind to membranes. U2OS cells stably expressing SNX10-EGFP WT, SNX10-EGFP Y32S or EGFP (control), were subjected to GFP-trap pulldown experiments, followed by analysis of their respective interactome by mass spectrometry. 53 proteins were identified as significant SNX10-EGFP interactors compared to control, out of which 29 proteins were specific for the WT versus the Y32S mutant and 24 were common (Fig. 3A). GO term analysis showed that these 53 proteins included proteins with predicted localization (Cellular component) to endomembrane compartments (e.g., LAMTOR1, SQSTM1, MVB12A), mitochondria (e.g., ATP5J, ATPIF1, COX-IV), endoplasmic reticulum (e.g., SERPINH1, TMEM109), and the extracellular space (e.g., YBX1, EEF1G). These proteins were associated with biological processes such as mitochondrial organization (e.g., COX-IV, UQCRFS1, SLC25A6), autophagy (e.g., LAMTOR1, GBA, SQSTM1), and endosome organization (e.g., SQSTM1, LAMTOR, MVB12A) (Fig. 3A-B).

Given the interaction of SNX10 with mitochondrial (e.g., COX-IV, ATP5J, ATPIF1), autophagic (e.g., SQSTM1/p62) and endolysosomal (e.g., MVB12A, LAMTOR1) proteins (Fig. 3A, B), as well as its localization to early and late endosomes, we speculated that SNX10 may function as a novel regulator of trafficking of mitochondrial material to or from the endolysosomal pathway. To

address this, U2OS SNX10-EGFP cells were labeled with MitoTracker Red and subjected to live cell imaging. Intriguingly, SNX10-EGFP-positive structures were found to localize near the mitochondrial network and move across mitochondria in a highly dynamic manner with occasional MitoTracker Red signal seen within SNX10 positive vesicles (Fig. 3C and Movie 1).

To assess whether mitochondria-associated SNX10-positive structures were induced upon induction of mitophagy, U2OS cells stably expressing SNX10-EGFP and mScarlet-RAB5 were treated or not for 24 hrs with deferiprone (DFP), an iron chelator known to trigger mitophagy in a HIF1a-dependent manner[32], then stained with MitoTracker Deep Red before live cell imaging. SNX10-EGFP and mScarlet-RAB5 positive vesicles containing mitochondrial material could be detected under basal conditions, and these became noticeably bigger upon DFP treatment (Fig. 3D). Intriguingly, there was a twofold increase in the expression of endogenous SNX10 mRNA in DFP treated cells (Supplementary Fig. 2B). Moreover, there was a significant increase in the co-occurrence of SNX10 positive structures with the autophagy membrane protein LC3B when treating the cells with DFP for 24 hrs. This was slightly reduced by inhibition of ULK1, a kinase required for autophagy initiation, using MRT[33] (Fig. 3F). Also, the co-occurrence of MitoTracker- and LC3B-positive structures with SNX10 increased with DFP and was only slightly reduced upon ULK1 inhibition, both under normal conditions and following a 24-hour DFP treatment (Fig. 3G). Taken together, our data suggest a role for SNX10 in mitophagy.

SNX10 regulates mitochondrial protein homeostasis

To decipher the nature of the mitochondrial cargo included in SNX10-positive vesicles, SNX10-EGFP cells were fixed and stained with antibodies against distinct mitochondrial proteins. Notably, incorporation of ATP5J, SAMM50, COX-IV, and TOMM20 into SNX10-EGFP vesicles was evident upon DFP treatment (Fig. 4A and Supplementary Fig. 3A), and more discreetly, TIMM23 and PDH (Supplementary Fig. 3B), although their mitochondrial staining was clear.

To further investigate whether SNX10 might regulate turnover of selected mitochondrial proteins, we assessed the abundance of mitochondrial proteins in cells transfected with control or SNX10 siRNA and treated or not with DFP for 24 hrs (Fig. 4B). Interestingly, SNX10 depletion seems to reduce the abundance of several mitochondrial proteins including TIMM23, PDH and COX-IV, both at basal levels and upon mitophagy induction, although only the effect on COX-IV levels was significant (Fig. 4C-E). Intriguingly, immunofluorescence staining for COX-IV revealed a strong reduction of staining intensity in cells depleted of SNX10, which was not recovered in

cells treated with the autophagy inhibitors IN1 (VPS34 inhibitor) or MRT (ULK1 inhibitor), indicating that SNX10-mediated reduction of COX-IV levels is independent of canonical autophagy (Fig. 4F). Moreover, using a pH-dependent mCherry-EGFP-tagged matrix reporter in U2OS cells[34] we did not see a significant effect of mitochondrial turnover upon SNX10 depletion (Supplementary Fig. 3C and D).

SNX10 regulates mitochondrial bioenergetics

To investigate whether the increased turnover of mitochondrial proteins seen upon SNX10 depletion could affect mitochondrial bioenergetics we first analyzed the level of citrate synthase activity, which is often used as a read-out for total mitochondrial levels[35], as citrate synthase catalyzes the first reaction of the Krebs cycle in the mitochondrial matrix. Indeed, the citrate synthase activity was decreased in SNX10 depleted cells compared to control cells, both under basal conditions and upon treatment with DFP for 24 hrs (Fig. 5A).

Given the interaction of SNX10 with ATP5J, a subunit of the mitochondrial ATP synthase (Fig. 3A) and its impact on the expression levels of key electron transport chain proteins (COX-IV) (Fig. 4A and B), we next investigated whether SNX10 depletion affected mitochondrial respiration. Indeed, SNX10 depletion decreased the baseline OCR (oxygen consumption rate; an indicator of mitochondrial respiration), and ATP-production linked respiration in U2OS cells, as analysed by a Seahorse XF Analyzer (Fig. 5B-D). Taken together, our data indicate that SNX10 is important for normal mitochondrial function and respiration.

SNX10 is partially conserved in zebrafish and expressed during early embryogenesis

To investigate a potential functional role of SNX10 *in vivo*, we employed zebrafish as a model system. Zebrafish contain SNX10 paralogues (snx10a and snx10b) that are ~60% similar to one another and ~59% homologous to human SNX10 with the N-terminal PX domain being the most highly conserved (~71% and ~63.5% respectively) (Fig. 6A). We first sought to examine the spatiotemporal expression pattern of snx10a and snx10b during the early development of zebrafish. While both snx10a and snx10b were consistently expressed from 1dpf to 5dpf as determined by real-time qPCR, snx10a transcripts were more abundant than snx10b transcripts (Fig. 6B), suggesting the importance of snx10a in the early development of the zebrafish larvae. Whole-mount in situ hybridization (WM-ISH) of snx10a and snx10b transcripts in 2dpf to 5dpf wild-type zebrafish larvae revealed expression of snx10a in the retina, optical tectum, intestine,

midbrain and hindbrain at all time points, whereas snx10b transcripts were found mainly in the retina and notochord at 2-5 dpf, and in the whole brain at 5dpf (Fig. 6C and supplementary Fig. 4A). There was no staining of the control sense probe at any time points.

SNX10 regulates degradation of IMM proteins in zebrafish

To explore a possible role for Snx10-regulated mitophagy in the early development of zebrafish larvae, we employed CRISPR/Cas9-mediated genome editing in zebrafish embryos using guide sequences targeting snx10a and snx10b individually or together (snx10ab double knockout (DKO)) (Supplementary Fig. 4B). The loss of Snx10 protein in DKO larvae compared to larvae injected with control oligo was verified via immunoblotting (Fig. 6D)

Control and snx10ab DKO larvae were treated with or without 100 µm DMOG (Dimethyloxalylglycine) for 24 hours at 2dpf to induce mitophagy[12], followed by immunoblotting to detect the inner mitochondrial membrane (IMM) proteins Cox-IV and Samm50 (Fig. 6E). As observed in U2OS cells, Cox-IV levels were reduced in snx10ab DKO larvae both at the basal level and upon DMOG treatment when compared controls (Fig. 6F). Samm50 levels were also reduced both in basal and induced conditions, although not significantly (Fig. 6G).

SNX10 affects cell death and oxidative stress in zebrafish

snx10ab DKO larvae showed a dysmorphic phenotype (data not shown) with most larvae exhibiting necrotic tissue damage in the head and trunk region, suggesting possible cell death. To investigate this, we performed TUNEL (terminal deoxynucleotidyl transferase dUTP nick end labelling) staining on sections of fixed control and snx10ab DKO larvae, treated with or without DMOG, followed by confocal microscopy and quantification of the mean fluorescent intensity in the region of interest (ROI) (Fig. 6H and I), the brain, since SNX10 expression was higher there. TUNEL staining showed increased cell death in snx10ab DKO larvae relative to control (Fig. 6I). Interestingly, DMOG treated control larvae also showed increased cell death as compared to untreated control larvae (Fig. 6I), which may suggest that increased turnover of mitochondria, caused by snx10 DKO or DMOG treatment, promotes cell death.

To assess whether the increased cell death seen in snx10 DKO larvae could be attributed to increased oxidative stress, trypsinized control and snx10ab DKO zebrafish larvae were treated with deep red MITOSOX dye and analyzed by FACS. Indeed, there was a significant increase in ROS levels in snx10ab DKO larval cells as compared to control (Fig. 6J and Supplementary Fig. 5C).

Taken together, our *in vivo* data show an important role for snx10 in preventing cell death and oxidative stress.

Discussion

In this manuscript we demonstrate that SNX10, a small PX domain protein, localize to early and late endocytic compartments in a PtdIns3P-dependent manner. We further show that SNX10 regulates trafficking in the endosomal pathway and that SNX10-positive endosomes dynamically interact with mitochondria to maintain mitochondria homeostasis and cellular bioenergetics.

Mutations in SNX10 are linked to autosomal recessive osteopetrosis (ARO)[18–21],a rare disease characterized by abnormally dense bone. Interestingly, all described ARO mutations in SNX10 are found in the PX domain[19–21], and we here show that three such mutants (Y32S, R51P and R51Q) fail to localize to endocytic compartments. The exact endosomal function of SNX10 is unclear, but we show that the large vacuoles formed upon SNX10 overexpression [31] were abolished upon expression of the ARO-linked PX mutants, in line with previous data showing that mutation of the predicted Ptdns3P binding residue of SNX10 (Arg/R[53]) prevents the formation of large vacuoles. Thus, it is likely that PtdIns3P-mediated endosome recruitment of SNX10 prevents ARO. However, as the ARO PX mutant used for interactome analysis in this study (Y23S) had more interactors than the WT SNX10, we cannot exclude the possibility that SNX10 PX mutants cause ARO through other mechanisms, e.g. through its C-terminal intrinsically disordered region (IDR), as IDRs generally are known for their dynamic and adaptable nature, existing in a repertoire of structurally distinct conformations that rapidly interconvert based on their cellular context[16]. Previous studies have linked the depletion of SNX10 to reduced maturation of CTSA (Cathepsin A), and increased levels of LAMP2A[36,37]. Thus, it is tempting to speculate that the large vacuoles observed upon SNX10 overexpression, could be caused by a downregulation of LAMP2A, leading to reduced fusion between late endosomes and lysosomes[38].

We found that SNX10 interacts with proteins belonging to the mitochondrial cell compartment and that depletion of SNX10 affects mitochondrial activity and protein levels, seemingly via promoting the degradation of mitochondrial proteins. Cells depleted of SNX10 displayed less mitochondrial abundance (reduced citrate synthase activity, a well-established marker for mitochondrial abundance[39]) and reduction of several mitochondrial markers, including proteins important for mitochondrial respiration, namely SAMM50 and COX-IV. Importantly, we also find that depletion of Snx10 in zebrafish leads to a reduction of Cox-IV and Samm50, indicating a

conserved role of Snx10 *in vivo* in the regulation of mitochondrial homeostasis. We observed staining of COX-IV within SNX10 and RAB5 positive vesicles were positive for LC3B, indicating a role for SNX10 in the regulation of mitophagy. However, the observed reduction of COX-IV and other mitochondrial proteins in SNX10-depleted cells seems partly independent of the core autophagy components VPS34 and ULK1, suggesting a non-canonical type of mitophagy. Cells lacking SNX10 displayed decreased mitochondrial respiration, which could explain the previously shown increase in glucose metabolism upon SNX10 depletion in intestinal epithelial cells[24].

Intriguingly, Snx10ab-depleted zebrafish larvae displayed necrotic tissue damage around the head region and showed increased cell death in the brain. Elevation of cell death in Snx10ab-depleted fish could be attributed to significantly high oxidative stress levels as ROS is a potent stimulus for cell death[40]. While decreased levels of mitophagy previously have been linked to increased ROS and cell death[41,42], we found that depletion of Snx10ab resulted in increased turnover of selected mitochondrial proteins and increased ROS and cell death in vivo. Also, induction of mitophagy using a hypoxia mimetic drug in control larvae significantly increased cell death, suggesting that excess mitophagy may trigger cell death[43].

Mitochondrial activity has been linked to lysosomal function[44–46] and emerging evidence shows that mitochondria interact with the endosomal compartment and that mitochondrial transfer happens between the two compartments[9,46]. Our data showing dynamic interactions of SNX10 with mitochondria may indicate a role for SNX10 in mitochondrial-endosome crosstalk beyond mitophagy, like the transportation of ions and metabolites such as iron and cholesterol[46]. Iron can be transferred directly from endosomes to mitochondria through a quick "kiss and run" interaction between these organelles that is influenced by endosomal iron levels[6–8]. Iron plays a crucial role in the proper functioning of respiratory complexes I-III in the mitochondrial electron transport chain. Interestingly, our observations revealed impaired mitochondrial respiration in SNX10-depleted cells, resulting in reduced oxygen consumption rate and ATP production, which may be linked to a role of SNX10 vesicles in delivering iron to mitochondria.

Dynamic interactions between mitochondria and endolysosomes have also been linked to pathogen killing by the transfer of mitochondrial ROS to phagosomes containing bacteria[47]. It is interesting to note that SNX10 has been related to pathologies connected to monocyte/macrophage malfunctioning[25,48]. Thus, SNX10 activity in the endolysosomal pathway is likely paramount for macrophage function and maturation[25], and their ability to kill bacteria[26].

In conclusion, we here present data that not only advances our understanding of SNX10's subcellular localization and regulatory roles in endocytosis but also uncovers a previously unknown interaction of SNX10 positive endosomes with mitochondria. This unexpected association opens avenues for exploring the intricate interplay between endocytic and mitochondrial pathways, emphasizing SNX10's crucial role in cellular homeostasis and providing a foundation for future investigations in both physiological and pathological contexts.

Materials and Methods

Antibodies and dyes

Primary antibodies used for immunoblotting: β-Actin (Cell Signaling Technology #3700, 1:5000), COX-IV (Cell Signaling Technology, #4850S, 1:1000), GAPDH (Abcam, Ab9484, 1:5000), GAPDH (Cell signaling, #5174, 1:1000) GFP (Takara, # 632569, 1:1000) EGFR (Fitzgerald, #20-ES04), P-EGFR (Tyr1068) (Cell Signaling, #3777, 1:1000), PDH (Cell Signaling Technology, #2784S, 1:1000), LC3B (Cell Signaling Technology, #3868, 1:1000), SNX10 (Atlas Antibodies, HPA015605, 1:1000), alpha Tubulin (GeneTex, GTX628802. 1:5000). Primary antibodies used for immunostaining: ATP5J (Atlas Antibodies, HPA031069, 1:200), Clathrin (Acris, #SM5011P), COX-IV (Cell Signaling Technology, #4850S, 1:1000), EEA1 (BD Biosciences, #610457; 1:250), LAMP1 (Santa Cruz Biotechnology, #sc-20011, 1:250), LC3B (MBL, #PM036, 1:250), SAMM50 (Novus Biologicals, NBP1-84509, 1:200), TIMM23 (BD Biosciences, # 611223, 1:250), TOMM20 (Santa Cruz, #17764, 1:200). Secondary antibodies used for immunoblotting: DyLight800 mouse and rabbit (Invitrogen, #SA5-10172 and #SA5-10044), StarBright Blue 700 mouse and rabbit (Bio-Rad, #12004158 and #12004161), Peroxidase AffiniPure™ Goat Anti-Mouse IgG (H+L) (Jackson, #115035003, #1:5000), Peroxidase AffiniPure™ Goat Anti-Rabbit IgG (H+L) (Jackson, #111035144, 1:5000). Fluorescent dyes used include: MitoTracker™ Deep Red FM (ThermoFisher, #M22425), MitoTracker™ Red CMXRos (ThermoFisher Scientific, #M7512), LysoTracker™ Red DND-99 (ThermoFisher # L7528), Hoechst 33342 (Invitrogen, #H1399).

Cell culture and reagents

U2OS TRex FlpIn cells (kindly provided by Steve Blacklow, Harvard Medical School, US) were used for generation of stable inducible cell lines. They were maintained in a complete medium of Dulbecco's Modified Eagle Medium (DMEM – Lonza 12-741F) supplemented with 10% fetal bovine serum (FBS – Sigma Aldrich #F7524), 100 U/ml penicillin and 100 µg/ml streptomycin

(ThermoFisher Scientific #15140122). Cells were kept in a humidified incubator at 37 °C and 5% CO_2.

For starvation conditions, the cells were incubated 2-4 hrs in Earle's balanced salt solution (EBSS; Gibco, # 24010043). Bafilomycin A1 (referred as BafA1, BML, #CM110) was used at 100 nM. Deferiprone (DFP; Sigma Aldrich, #379409) was used at 1 mM. Doxycycline (Clontech, #631311) was used at 100 ng/ml. EGF VPS34-IN1 (Selleckchem, # S7980) was used at 5 µM.

Cell transfection

For the generation of stable cell lines U2OS FlpIn TRex cells were transfected with pcDNA5/FRT/TO-SNX10-EGFP wild type or mutant constructs (Table 1) using Lipofectamine 2000 (Invitrogen, #11668019). Positively transfected cells were selected with hygromycin B (EMD Millipore, #400052). Doxycycline was used at 100 ng/ml for 24 hrs to induce protein expression. Cell lines expressing mScarlet-tagged RAB proteins were created with lentiviral transduction. Briefly, 293FT cells were co-transfected with psPAX2 and pCMV-VSVG plasmids to generate lentiviral particles. These particles were transduced, after harvesting and filtering, into the SNX10-EGFP stable cell line together with 10 ug/ml polybrene (Santa Cruz, sc-134220) and selected using puromycin (Sigma #P7255). The plasmids used for the cell lines creation are compiled in Table 1. Point mutations were introduced by using the QuickChange site-directed mutagenesis kit (Agilent Technologies) and the primers used for this are listed in Table 1.

For siRNA transfections, cells were incubated with Silencer Select siRNA oligonucleotides targeting each gene at 20 nM, in combination with RNAiMAX (Invitrogen, #13778150) through reverse transfection. The cells were fixed/harvested for further procedures after 72 hrs of knockdown.

Citrate Synthase Assay

Biochemical quantification of mitochondrial abundance was done by analysis of citrate synthase activity. Briefly, U20S cells were plated and grown as described in the figure legend. The cells were harvested after washing twice with PBS on ice and then lysed in NP-40 lysis buffer (50 mM HEPES pH 7.4, 150 mM NaCl, 1 mM EDTA, 10% (v/v) NP-40 + 1 mM DTT, it also contained 1x Phosphatase inhibitors and 1x Protease inhibitors added fresh). Cell lysates were centrifuged at 21000 x g for 10 min at 4ºC and the supernatant was obtained. The protein concentration was quantified by Bradford assay. To determine the citrate synthase activity, 0.4 µl of cell lysate was

added to 198 µl of CS assay buffer (100 mM Tris pH 8, 0.1% Triton X-100, 0.2 mM DTNB (5,5'Dithiobis (2-nitrobenzoic acid)), 0,1mM Acetyl CoA). At the starting point, 2µl of 20 mM Oxaloacetate was added and the plate was incubated at 35ºC. The reactions were monitored in a FLUOstar OPTIMA plate reader (BMG Labtech) at λ_{Abs}= 440 nm. The reactions were scanned each 87s for a total of 40 cycles. The values were compared to the Oxaloacetate lacking controls. The rate of the reactions was plotted to determine the citrate synthase activity and the activity rate was calculated using the linear part of the curve, before saturation was reached. Then the values were normalized to protein concentration and then normalized to control value. The graph displays relative values.

Immunofluorescence

The cells were seeded onto glass coverslips or 96 well plates for high-throughput imaging. siRNA treatment lasted for 72 hrs and stable cell lines were subjected to doxycycline for 24 hrs prior to treatments to allow protein expression, as indicated in figure legends. After treatments, the cells were washed with PBS and then fixed with PFA fixation buffer (3.7% (w/v) PFA, 200mM HEPES pH 7.0) for 20 min. After fixing, the cells were washed twice with PBS and then permeabilised for 5 min with 0.2% (v/v) NP-40 in PBS. Cells were then washed once and then incubated for blocking for 15 min with 1% BSA in PBS solution (IF blocking solution). After blocking, the coverslips were incubated with the primary antibodies for 1 hr at 37 °C (antibodies were diluted IF blocking solution at the dilutions stated in the section "Antibodies and dyes") and then washed 3x10 min in IF blocking solution. After washing the cells were incubated with their corresponding secondary antibodies again diluted in IF blocking solution at the concentrations above stated, for 30 min at room temperature (RT). Finally, the cells were washed again with IF blocking solution and then incubated with Hoechst 33342 diluted in 1xPBS at 1µg/ml for 30 min. Coverslips were mounted in ProLong Diamond Antifade Mountant (Invitrogen, #p36965).

Live-cell imaging, high content immunofluorescence microscopy and confocal microscopy.

Imaging settings (laser intensity, time exposure, number of sections per z-stack and the stepsize between them, time intervals during live imaging) were set identically within each experiment to allow an optimal and non-saturated fluorescent imaging. For widefield imaging we used an ImageXpress Micro Confocal microscope from Molecular devices at 20x magnification. Live imaging and imaging of fixed cells were acquired using a Dragonfly 505 spinning disk confocal

microscope (Andor Technology) utilizing a 63x or 100x oil objective. If any other microscope was used, it will be specified in the figure legend.

Oxygen consumption rate measurement

SNX10 was depleted as described above for a total of 72 hrs. Prior starting the experiment, the cells were resuspended in complete DMEM and seeded into Seahorse XFe24 Cell Culture microplates where they reached confluency. The plate was incubated at 37 °C in a humidified incubator. The media was then replaced with DMEM without Sodium Bicarbonate (pH 7.4) before analysis with the Seahorse XFe24 Analyzer (XF mito stress test, Agilent). Specific mitochondrial inhibitors were dissolved in DMEM and loaded into the injector ports of the Seahorse Sensor Plates. The final concentrations of the mitochondrial inhibitors were: CCCP: 1 µM, Oligomycin: 1.5 µM, Rotenone: 0.5 µM, Antimycin A: 0.5 µM. After the analysis, the cells were washed in ice cold PBS and lysed with NP-40 lysis buffer for protein quantification using BCA Assay (Thermo Fisher). Quantification was performed using the Seahorse Analytics software (seahorseanalytics.agilent.com, Agilent), with normalization based on the measured protein concentration from each well.

RNA Isolation, cDNA synthesis and qPCR

For quantifying the knockdown efficiency throughout the different experiments, RNA was isolated using the RNeasy Plus Mini Kit (Qiagen), except for RNA from experiments containing DFP, that was isolated using Trizol (ThermoFisher Scientific, #15596026). cDNA was synthesized using Superscript III reverse transcriptase (ThermoFisher Scientific, #18080085), and amplified using KAPA SYBR FAST qPCR Kit and designed primers targeting specific genes. For experiments performed in a 96 well format the Power SYBR Green Cells-to-CT kit (ThermoFisher Scientific, #4402955) was used for extraction and amplification according to manufacturer's instructions. All amplification experiments were run in a CFx96 real-time PCR system (Bio-Rad). Transcript levels were normalized to TATA-box-binding protein (TBP) and the quantifications were performed using the $2^{-\Delta\Delta Ct}$ method. The primers used for real time PCR in this study are: SNX10: 5'TTGAGGCGTGTGTTTCTGGG3' (fwd), and 5'CCAAGCCCAGAGGATGAACTTT3' (rev). TBP: 5 CAGAAAGTTCATCCTCTGGGCT3' (fwd), and 5' TATATTCGGCGTTTCGGGCA3' (rev). 'ULK1: 5'GTTCCAAACACCTCGGTCCT3' (fwd), and 5'TCCACCCAGAGACATCTTCCT3'.

Correlative light and electron microscopy

For CLEM, U2OS FlpIn cells, stably expressing SNX10-EGFP were seeded on photo-etched coverslips (Electron Microscopy Sciences, Hatfield, USA). Cells were fixed in 4% formaldehyde, 0.1% glutaraldehyde in 0.1 M PHEM (240 mM PIPES, 100 mM HEPES, 8 mM MgCl2, 40 mM EGTA), pH 6.9, for 1 hr. The coverslips were washed with 0.1M PHEM buffer and mounted with Mowiol containing 1µg/ml Hoechst 33342. The cells were examined with a Dragonfly 505 spinning disk confocal microscope (Andor Technology) using an oil immersed 60x magnification objective. Cells of interest were identified by fluorescence microscopy and a Z-stack covering the whole cell volume was acquired. The relative positioning of the cells on the photo-etched coverslips was determined by taking a low magnification DIC image. The coverslips were removed from the object glass, washed with 0.1 M PHEM buffer and fixed in 2% glutaraldehyde/0.1 M PHEM overnight. Cells were postfixed in osmium tetroxide and potassium ferry cyanide, stained with tannic acid, and uranyl acetate and thereafter dehydrated stepwise to 100% ethanol followed by flat-embedding in Epon. Serial sections (200nm) were cut on a Ultracut UCT ultramicrotome (Leica, Germany) and collected on formvar coated slot-grids.

Sections were observed at 200 kV in a Thermo ScientificTM TalosTM F200C microscope and recorded with a Ceta 16M camera. For tomograms, image series were taken between -60° and 60° tilt angles with 2° increment. Single-axes tilt series were recorded with a Ceta 16M camera. Tomograms were computed using weighted back projection using the IMOD package. Display, segmentation and animation of tomograms were also performed using IMOD software version 4.9.[49]

To assess the diameter of endosomes, U2OS cells subjected to SNX10 silencing were grown on poly-l-lysine coated sapphire discs. To label newly internalized EGFR following EGF-stimulation, cells were first washed in ice cold PBS and incubated with an antibody recognizing the extracellular part of EGFR (mouse anti-EGFR, Pharmingen) on ice. After washing four times with ice cold PBS, cells were incubated with Protein A-10 nm gold conjugate (UMC Utrecht Dept. of Cell Biology) which recognizes the Fc region of the mouse IgG2b primary antibody. Cells were again washed four times with ice cold PBS, stimulated with EGF in warm DMEM for 40 min and finally high pressure frozen using a Leica HPM100. Freeze substitution was performed as follows: sample carriers designed for sapphire discs were filled with 4 ml of freeze substituent (0.1% (w/v) uranyl acetate in acetone, 1% H2O) and placed in a temperature-controlling AFS2 (Leica) equipped with an FPS robot. Freeze-substitution occurred at -90ºC for 48 hrs before the

temperature was raised to -45 °C over a time span of 9 hrs. The samples were kept in the freeze substituent at -45 °C for 5 hrs before washing 3 times with acetone followed by a temperature increase (5 °C per hour) to -35 °C. Samples were stepwise infiltrated with increasing concentrations of Lowicryl HM20 (10%, 25%, 75%, 4 hrs each). During the last two steps, the temperature was gradually raised to -25°C before infiltrating 3 times with 100% Lowicryl (10 hrs each). Subsequent UV-polymerization was initiated for 48 hrs at -25 °C, and the temperature was then evenly raised to +20 °C (5 °C per hour). Polymerization then continued for another 24 hrs at 20 °C. Serial sections (250 nm) were cut on an Ultracut UCT ultramicrotome (Leica, Germany) and collected on formvar coated slot grids.

Single-axis tilt tomograms were collected in a Thermo ScientificTM TalosTM F200C microscope equipped with a with a Ceta 16M camera and image series were taken between -60° and 60° tilt angles with 2° increment. Tomograms were reconstructed using weighted back projection using the IMOD package software version 4.9[49].

Proteomics and bioinformatics

To analyse the SNX10-EGFP interactome we used mass spectrometry assays. U2OS cells expressing SNX10-EGFP wild type or the Y32S mutant were subjected to GFP pulldown using the ChromoTek GFP-Trap®, following the vendor's specifications. The mass spectrometry experiments were performed at the Proteomics Core Facility at Oslo University Hospital (Rikshospitalet). The analysis of label free intensities was performed with Perseus[50]. We used R (R Core Team, 2020)[51] limma[52] for performing imputation of missing values and fold change analysis. The proteins with contaminants were omitted from the analysis. Piecharts and Venn diagrams were plotted using ggplot2 R package and InteractiVenn[53], respectively. The experimental values were statistically analyzed using GraphPad Prism.

Western blotting

For western blotting, the cells were treated as indicated in each experiment and then moved onto ice prior lysing. Briefly, the cells were washed twice with PBS and then lysed on ice in NP-40 lysis buffer (50mM HEPES pH 7.4, 150mM NaCl, 1mM EDTA, 10% Glycerol, 0.5% NP-40) supplemented with protease and phosphatase inhibitors (unless specified otherwise). The cells were incubated for 10 min and then collected. The samples were then centrifuged at 21000xg at 4°C during 10 min and then the supernatant was collected. Protein quantitation was assessed by

Bradford assay (Bio-Rad #5000006) using serial dilutions of bovine serum albumin (BSA) as standards. Samples were then normalized and added to sample buffer (2.8x NuPage LDS Sample buffer + DTT 0.30M). After running the samples by an SDS polyacrylamide gradient gel (4–20% Criterion™ TGX™ Precast Midi Protein Gel, Bio-Rad) and transferring them to a PVDF membrane (350mA/1h), the samples were blocked with casein buffer (0.5% Casein, 0.1%, NaAzide, PBS) for 1h at RT and then incubated overnight at 4°C with primary antibodies. Primary antibodies were diluted in a 5% BSA in PBST solution (1X Phosphate-Buffered Saline, 0.1% Tween® 20 Detergent). Membranes were washed 3x10 min in PBST and then incubated with the secondary antibodies 1h at RT. Membranes were washed again 3x10 min in PBST and a last wash in PBS prior image acquisition with an Odyssey CLx Infrared Imaging system. For HRP-conjugated secondary antibodies, the membranes were developed using the ECL kit and scanned with ChemiDoc MP Imaging system (Bio-Rad). The blots were quantified with Image Studio Lite software and GraphPad Prism were used for statistical analysis (unpaired t test) of the data.

Whole-mount in situ hybridization (WM-ISH)

Whole-mount in situ hybridizations for snx10a and snx10b were performed as previously described (Thisse and Thisse, 2008) using digoxigenin-labelled riboprobes. Primer sequences for snx10a sense and antisense probes were; ATG probe: forward primer (5' ATGGATAACACAAGCTTTGAG3'), reverse primer (5'TCATATAACTGAATGGCCATG3') and for snx10b sense and antisense probes were; ATG probe: forward primer (5'TATGCAGGAATTCACTGGCG3'), reverse primer (5' CACTCTGATTCACATTGCAC3')

EGF treatment

U2OS FlpIn TRex pcDNA5-SNX10-EGFP cells transfected with control or SNX10 siRNA for 72 hours were then serum starved for 2 hrs in media supplemented with 10 µg/ml Cycloheximide, followed by addition of 50 ng/ml EGF (Santa Cruz Biotechnology, sc-4552) in combination with 10 µg/ml Cycloheximide (Sigma, C7698) for 0, 20 and 60 min. The cells were harvested at selected time points and lysed for 10 min on ice in lysis buffer (50 mM Tris pH 8.0, 1 mM EDTA, 2% SDS, supplemented with protease and phosphatase inhibitor cocktails). Next, the lysates were boiled for 10 min at 70°C and sonicated in a waterbath sonicator at 4°C (2 x 10 cycles (30 sec on, 30 sec off) Bioruptor Pico, Diagenode).

Zebrafish Maintenance

Wild-type zebrafish (AB strain) were housed at the zebrafish facility at the Centre for Molecular Medicine Norway (AVD.172) using standard practices. Embryos were incubated in egg water (0.06 g/L salt (Red Sea)) or E3 medium (5 mM NaCl, 0.17 mM KCl, 0.33 mM CaCl2, 0.33 mM MgSO4, equilibrated to pH 7.0). Embryos were held at 28 °C in an incubator following collection. Experimental procedures followed the recommendations of the Norwegian Regulation on Animal Experimentation ("Forskrift om forsøk med dyr" from 15.jan.1996). All experiments conducted on wild-type zebrafish larvae were done at 5 dpf or earlier.

CRISPR/Cas9 genome editing in zebrafish

Zebrafish snx10a and snx10b knock-out embryos were generated using CRISPR/Cas9 technology as described (Kroll et al., 2021). Two guide RNA's were designed each for snx10a and snx10b respectively, based on predictions from the online sgRNA prediction web tool CHOPCHOP (http://chopchop.cbu.uib.no/index.php). Genomic DNA sequences retrieved from Ensembl GRCz10 or z11 (http://uswest.ensembl.org/Danio_rerio/Info/Index) were used for the target site searches. The two guides, designated as sgRNA#1 and sgRNA#2, were predicted to target exon 2 and exon 3 of the snx10a gene and exon 1 and 3 of the snx10b gene respectively. sgRNA is the annealed product of a target specific element called the crRNA and trans-activating CRISPR element called tracrRNA (both of which are ordered from Integrated DNA technologies, IDT). 1 ul of each of these nucleotide elements were annealed together with 1.28 ul of duplex buffer in a thermocycler at 95 ^{o}C for 5 min. Post annealing, 1 ul of sgRNA and 1 ul of Cas9 nuclease (IDT) was incubated together in a thermocycler at 37 ^{o}C for 5 min. sgRNA assembled with Cas9 is RNP. snx10a RNP was pooled together with snx10b RNP to create a mix of snx10ab RNP to create double knock-outs. 1nl (267.5 pg) of this mix was injected in the yolk sac at the single cell stage before the cell inflated. Oligonucleotides used for snx10a sgRNA synthesis were sgRNA#1 (5'ACGGGAUCCUCAGGUUCACAGUUUUAGAGCUAUGCU3') and sgRNA#2 (GGGUUCCAAGGAGGAAGUUUGUUUUAGAGCUAUGCU); for snx10b sgRNA synthesis were sgRNA#1 (5' AGAAAUUGGAGCCCGUAUGGGUUUUAGAGCUAUGCU3') and sgRNA#2 (5' CAUGCCAGAAAUCUUCCUUCGUUUUAGAGCUAUGCU3'). TracrRNA used was (5'AAAAGCACCGACTCGGTGCCACTTTTTCAAGTTGATAACGGACTAGCCTTA TTTTAACTTGCTATTTCTAGCTCTAAAAC'3).

Zebrafish cryosectioning, cell death assay by TUNEL Staining, confocal microscopy and image analysis

Control and *snx10ab* double knock-out (DKO) zebrafish larvae were treated with or without (just DMSO) 100 uM DMOG for 24 hours. At experimental endpoints, larvae were washed once in embryo water and fixed with 4% PFA (in HEPES) at RT for 2 hours. Post fixation, larvae were washed three times in PBS. The larvae were then cryopreserved in a 2 mL tube in increasing amounts of sucrose in 0.1 M PBS with 0.01% sodium azide. Cryopreservation was done first in 15% sucrose solution for 1 hr at RT or up until larvae dropped to the bottom of the tube and then in 30% sucrose solution at 4 °C overnight with gentle shaking. Cryopreserved larvae were oriented in a cryomold (Tissue-Tek Cryomold, Sakura, Ref: 4565) with optimal cutting temperature compound (OCT compound, Tissue-Tek Sakura, Ref: 4583). Larvae were oriented with the ventral side down, and additional OCT was added to fill the mold and frozen on dry ice. A solid block of OCT with larvae oriented in the desired way was taken out from the mold and 12-µm coronal slices were sectioned on a cryostat (Thermo Scientific). Sections were collected on Superfrost Plus glass slides (Thermo Scientific, Ref: J1800AMNZ) and kept at RT for at least 2 hrs to firmly tether slices onto the glass slide.

Slides were rehydrated three times in PBS at room temperature for 3 min each. The area of interest was circled by a hydrophobic PAP pen (Abcam, ab2601), and the slides were placed in a humidified chamber to avoid drying out. Rest of the procedure for TUNEL staining (Terminal deoxynucleotidyl transferase-mediated deoxyUridine triphosphate Nick-End Labeling; Thermo Fisher Scientific) was performed according to the manufacturer's instructions. Confocal images were obtained using an Apochromat ×20/0.8 or ×40/1.0 oil DIC objective on an LSM 800 microscope (Zeiss). Image analysis was performed using Fiji by which mean fluorescent intensity was measured in the brain region of the respective sections of zebrafish larvae.

ROS analysis in Zebrafish

The analysis of reactive oxygen species (ROS) levels in zebrafish was performed as described [54]. Briefly, after dissociation into single cells of the respective larvae, cells were treated with 5 µM of MitoSOX (Thermo Fisher Scientific) in Hanks Balanced Salt Solution (HBSS) for 15 min at 28°C in the dark. Cells were then centrifuged for 5 min at 250 x g at 4 °C, the supernatant discarded, and the cells washed with HBSS. FACS estimations were done on NovoCyte Flow Cytometer Systems, using an excitation peak of 396-nm for selective detection of mito superoxide.

Statistics

Experimental values were used for statistical analysis using Prism (v8.0.1) where indicated using analyses and post-hoc tests as indicated in figure legends. All data values come from distinct samples. Where shown **** = p>0.0001, *** = p >0.001, ** = p>0.01, * = p > 005 or n.s = not significant.

Online Supplemental material

Fig. S1 shows additional data for Fig. 1. Fig. S2 shows additional data for Fig. 3. Fig. S3 shows additional data for Fig. 4 and 5. Fig. S4 shows additional data for Fig. 6. Table S1 includes plasmids used in this study. Movie 1 is the time-lapse video of the data shown in Fig. 3C.

Data availability

All data used in this study are available upon request.

Acknowledgements:

We would like to thank the Simonsen lab for their support and critical discussion throughout the project development as well as Ulrikke Dahl Brinch for assistance with EM sample preparation. We acknowledge the Norwegian Core Facility for Human Pluripotent Stem Cells at the Norwegian Center for Stem Cell Research for mycoplasma testing and the ALM core facility, Gaustad node, where high-content imaging was performed. This project was carried out with funding from the Norwegian Cancer Society (grants no. 171318 and 223278), from the European Union's Horizon 2020 research and innovation program under the Marie Skłodowska-Curie (grant no. 801133), the South-Eastern Norway Regional Health Authority (grant no. 2020032) and the Research Council of Norway through its Centers of Excellence funding scheme (grant no. 262652) and FRIPRO (grant no. 249753).

Author contributions: LTM and AS designed and conceptualized the research project. AS supervised the work. LTM carried out most in vitro experiments. CV and NTA contributed performing experiments. BJM Performed all *Danio rerio* experiments. AL and SP contributed to cloning design and molecular biology. SS analyzed mass spectrometry and proteomics data. SWS performed the electron microscopy experiments. LTM and AS analyzed the data and wrote the manuscript.

References

1. Vagnozzi, A. N. & Praticò, D. Endosomal sorting and trafficking, the retromer complex and neurodegeneration. *Molecular Psychiatry* vol. 24 857–868 at https://doi.org/10.1038/s41380-018-0221-3 (2019).
2. Feng, Y., He, D., Yao, Z. & Klionsky, D. J. The machinery of macroautophagy. *Cell Research* vol. 24 24–41 at https://doi.org/10.1038/cr.2013.168 (2014).
3. Melia, T. J., Lystad, A. H. & Simonsen, A. Autophagosome biogenesis: From membrane growth to closure. *Journal of Cell Biology* vol. 219 at https://doi.org/10.1083/JCB.202002085 (2020).
4. Hyttinen, J. M. T., Niittykoski, M., Salminen, A. & Kaarniranta, K. Maturation of autophagosomes and endosomes: A key role for Rab7. *Biochim. Biophys. Acta - Mol. Cell Res.* **1833**, 503–510 (2013).
5. Rusten, T. E. & Stenmark, H. How do ESCRT proteins control autophagy? *J. Cell Sci.* **122**, 2179–2183 (2009).
6. Das, A., Nag, S., Mason, A. B. & Barroso, M. M. Endosome-mitochondria interactions are modulated by iron release from transferrin. *J. Cell Biol.* **214**, 831–845 (2016).
7. Hamdi, A. *et al.* Erythroid cell mitochondria receive endosomal iron by a “kiss-and-run” mechanism. *Biochim. Biophys. Acta - Mol. Cell Res.* **1863**, 2859–2867 (2016).
8. Sheftel, A. D., Zhang, A. S., Brown, C., Shirihai, O. S. & Ponka, P. Direct interorganellar transfer of iron from endosome to mitochondrion. *Blood* **110**, 125–132 (2007).
9. Hammerling, B. C. *et al.* A Rab5 endosomal pathway mediates Parkin-dependent mitochondrial clearance. *Nat. Commun.* **8**, (2017).
10. Yamano, K. *et al.* Endosomal rab cycles regulate parkin-mediated mitophagy. *Elife* **7**, (2018).
11. Shutt, T. E. & McBride, H. M. Staying cool in difficult times: Mitochondrial dynamics, quality control and the stress response. *Biochim. Biophys. Acta - Mol. Cell Res.* **1833**, 417–424 (2013).
12. Munson, M. J. *et al.* GAK and PRKCD are positive regulators of PRKN-independent mitophagy. *Nat. Commun.* **12**, (2021).
13. Chandra, M. *et al.* Classification of the human phox homology (PX) domains based on their phosphoinositide binding specificities. *Nat. Commun.* **10**, (2019).
14. Jumper, J. *et al.* Highly accurate protein structure prediction with AlphaFold. *Nature* **596**, 583–589 (2021).
15. Varadi, M. *et al.* AlphaFold Protein Structure Database: Massively expanding the structural coverage of protein-sequence space with high-accuracy models. *Nucleic Acids Res.* **50**, D439–D444 (2022).
16. Holehouse, A. S. & Kragelund, B. B. The molecular basis for cellular function of intrinsically disordered protein regions. *Nat. Rev. Mol. Cell Biol.* (2023) doi:10.1038/s41580-023-00673-0.
17. Chen, Y. *et al.* A SNX10/V-ATPase pathway regulates ciliogenesis in vitro and in vivo. *Cell Res.* **22**, 333–345 (2012).
18. Pangrazio, A. *et al. SNX10* mutations define a subgroup of human autosomal recessive osteopetrosis with variable clinical severity. *J. Bone Miner. Res.* **28**, 1041–1049 (2013).
19. Amirfiroozy, A. *et al.* A Novel Mutation in SNX10 Gene Causes Malignant Infantile Osteopetrosis. *Avicenna J. Med. Biotechnol.* **9**, 205–208 (2017).

20. Koçak, G. *et al.* TCIRG1 and SNX10 gene mutations in the patients with autosomal recessive osteopetrosis. *Gene* **702**, 83–88 (2019).

21. Stattin, E.-L. *et al.* SNX10 gene mutation leading to osteopetrosis with dysfunctional osteoclasts. *Sci. Rep.* **7**, 3012 (2017).

22. Deng, R. rong & Yuan, Y. ping. Ropivacaine inhibits the proliferation and metastasis of gastric cancer cells via the SNX10/SRC/STAT3 pathway. *Chem. Biol. Drug Des.* **103**, 1–10 (2024).

23. Gimple, R. C. *et al.* Sorting nexin 10 sustains PDGF receptor signaling in glioblastoma stem cells via endosomal protein sorting. *JCI Insight* **8**, 1–25 (2023).

24. Feng, H. *et al.* α-hederin regulates glucose metabolism in intestinal epithelial cells by increasing SNX10 expression. *Phytomedicine* **111**, 154677 (2023).

25. You, Y. *et al.* Sorting nexin 10 acting as a novel regulator of macrophage polarization mediates inflammatory response in experimental mouse colitis. *Sci. Rep.* **6**, 20630 (2016).

26. Lou, J. *et al.* SNX10 promotes phagosome maturation in macrophages and protects mice against Listeria monocytogenes infection. *Oncotarget* **8**, 53935–53947 (2017).

27. Bao, W. *et al.* Inhibiting sorting nexin 10 promotes mucosal healing through SREBP2-mediated stemness restoration of intestinal stem cells. *Sci. Adv.* **9**, (2023).

28. Hansen, G. T. *et al.* Genetics of sexually dimorphic adipose distribution in humans. *Nat. Genet.* **55**, 461–470 (2023).

29. Elson, A. *et al.* Sorting Nexin 10 as a Key Regulator of Membrane Trafficking in Bone-Resorbing Osteoclasts: Lessons Learned From Osteopetrosis. *Front. Cell Dev. Biol.* **9**, 1–17 (2021).

30. Simonsen, A. *et al.* EEA1 links PI(3)K function to Rab5 regulation of endosome fusion. *Nature* **394**, 494–498 (1998).

31. Qin, B., He, M., Chen, X. & Pei, D. Sorting nexin 10 induces giant vacuoles in mammalian cells. *J. Biol. Chem.* **281**, 36891–6 (2006).

32. Allen, G. F. G., Toth, R., James, J. & Ganley, I. G. Loss of iron triggers PINK1/Parkin-independent mitophagy. *EMBO Rep.* **14**, 1127–35 (2013).

33. Petherick, K. J. *et al.* Pharmacological inhibition of ULK1 kinase blocks mammalian target of rapamycin (mTOR)-dependent autophagy. *J. Biol. Chem.* **290**, 11376–11383 (2015).

34. Princely Abudu, Y. *et al.* NIPSNAP1 and NIPSNAP2 Act as “Eat Me” Signals for Mitophagy. *Dev. Cell* **49**, 509-525.e12 (2019).

35. Shepherd, D. & Garland, P. B. The kinetic properties of citrate synthase from rat liver mitochondria. *Biochem. J.* **114**, 597–610 (1969).

36. You, Y. *et al.* SNX10 mediates alcohol-induced liver injury and steatosis by regulating the activation of chaperone-mediated autophagy. *J. Hepatol.* **69**, 129–141 (2018).

37. Lee, W. *et al.* SNX10-mediated degradation of LAMP2A by NSAIDs inhibits chaperone-mediated autophagy and induces hepatic lipid accumulation. *Theranostics* **12**, 2351–2369 (2022).

38. Hubert, V. *et al.* LAMP-2 is required for incorporating syntaxin-17 into autophagosomes and for their fusion with lysosomes. *Biol. Open* **5**, 1516–1529 (2016).

39. Larsen, S. *et al.* Biomarkers of mitochondrial content in skeletal muscle of healthy young human subjects. *J. Physiol.* **590**, 3349–3360 (2012).

40. Simon, H. U., Haj-Yehia, A. & Levi-Schaffer, F. Role of reactive oxygen species (ROS) in apoptosis induction. *Apoptosis* **5**, 415–418 (2000).

41. Baechler, B. L., Bloemberg, D. & Quadrilatero, J. Mitophagy regulates mitochondrial network signaling, oxidative stress, and apoptosis during myoblast differentiation. *Autophagy* **15**, 1606–

1619 (2019).

42. Lin, Q. *et al.* PINK1-parkin pathway of mitophagy protects against contrast-induced acute kidney injury via decreasing mitochondrial ROS and NLRP3 inflammasome activation. *Redox Biol.* **26**, 101254 (2019).

43. Ma, L., Han, T. & Zhan, Y. Mechanism and role of mitophagy in the development of severe infection. *Cell Death Discov.* **10**, 88 (2024).

44. Baixauli, F. *et al.* Mitochondrial respiration controls lysosomal function during inflammatory t cell responses. *Cell Metab.* **22**, 485–498 (2015).

45. Todkar, K., Ilamathi, H. S. & Germain, M. Mitochondria and lysosomes: Discovering bonds. *Frontiers in Cell and Developmental Biology* vol. 5 106 at https://doi.org/10.3389/fcell.2017.00106 (2017).

46. Todkar, K., Chikhi, L. & Germain, M. Mitochondrial interaction with the endosomal compartment in endocytosis and mitochondrial transfer. *Mitochondrion* vol. 49 284–288 at https://doi.org/10.1016/j.mito.2019.05.003 (2019).

47. Abuaita, B. H., Schultz, T. L. & O'Riordan, M. X. Mitochondria-Derived Vesicles Deliver Antimicrobial Reactive Oxygen Species to Control Phagosome-Localized Staphylococcus aureus. *Cell Host Microbe* **24**, 625-636.e5 (2018).

48. Lou, J. *et al.* SNX10 promotes phagosome maturation in macrophages and protects mice against Listeria monocytogenes infection. *Oncotarget* **8**, 53935–53947 (2017).

49. Kremer, J. R., Mastronarde, D. N. & McIntosh, J. R. Computer visualization of three-dimensional image data using IMOD. *J. Struct. Biol.* **116**, 71–76 (1996).

50. Tyanova, S. *et al.* The Perseus computational platform for comprehensive analysis of (prote)omics data. *Nature Methods* vol. 13 731–740 at https://doi.org/10.1038/nmeth.3901 (2016).

51. Team, R. C. R: The R Project for Statistical Computing. https://www.r-project.org/ (2020).

52. Ritchie, M. E. *et al.* Limma powers differential expression analyses for RNA-sequencing and microarray studies. *Nucleic Acids Res.* **43**, e47 (2015).

53. Heberle, H., Meirelles, V. G., da Silva, F. R., Telles, G. P. & Minghim, R. InteractiVenn: A web-based tool for the analysis of sets through Venn diagrams. *BMC Bioinformatics* **16**, 1–7 (2015).

54. Mugoni, V., Camporeale, A. & Santoro, M. M. Analysis of oxidative stress in Zebrafish embryos. *J. Vis. Exp.* 1–11 (2014) doi:10.3791/51328.

Author notes

Disclosures: The authors declare no competing interests exist.

Figure legends

Figure 1. SNX10 localizes to early and late endocytic compartments

A) SNX10 graphical view. The PX domain is represented in green, and the arrows indicate the position of the natural variants (SNPs) linked to ARO (R16L, Y32S, R51P, R51Q). **B)** Confocal imaging of U2OS cell lines stably expressing doxycycline inducible SNX10-EGFP WT or the indicated ARO-linked mutants. Nuclei were stained with Hoechst. Scale bar = 20µm. **C)** Representative immunoblot showing the expression levels of SNX10-EGFP and the indicated ARO mutants. The membrane was blotted using and antibody anti GFP and using Actin as loading control. **D and E)** Representative immunofluorescence images of U2OS cells stably expressing SNX10-EGFP WT or the Y32S mutant (green) immuno-stained with anti-EEA1 (D) or anti-LAMP1 antibodies (E) (magenta) after treating cells with 5µM VPS34-IN1 for 2h. Nuclei were stained with Hoechst. Scale bar = 10µm **F)** U2OS cells with stable inducible expression of SNX10-EGFP were infected with lentiviral particles to express mScarlet-RAB5/RAB7/RAB9 vectors. Nuclei were stained with Hoechst. Scale bars, 10 µm. **G)** U2OS SNX10-EGFP cells fixed for CLEM analysis. The area analyzed and showed in (ii) is indicated with a square in the confocal image (i). (iii) shows the transmission EM and (iv) the z-slide from the tomogram. The white arrows indicate clathrin coated vesicles. (v) green: endosomes; red: lipid droplets; yellow: vesicles; and pink: clathrin coated vesicles Scale bars, 10 µm (i and ii), 1 µm (iii and iv).

Figure 2. SNX10 regulates endocytic trafficking

A) Graphical description of the plasma membrane EGFR staining. Live cells are put on ice, and (1) incubated for 20 min with the primary anti-EGFR antibody, then washed and (2) incubated with a secondary antibody for 20 min, followed by (3) incubation with EGF for 15 or 50 min at 37°C before fixation and imaging. **B)** U2OS SNX10-EGFP cells were incubated with anti EGFR antibody as described in A), then stimulated with EGF and fixed. Cells were stain with an anti-EFG antibody after fixation. Scale bar: 10µm. **C)** After 72 h of siRNA transfection, U2OS SNX10-EGFP cells were serum starved for 2 h and then incubated with 50 ng/ml EGF + 10 µg/ml Cycloheximide (CHX) for the indicated times. The cells were lysed followed by western blotting for the indicated proteins. **D)** Quantification of EGFR and pEGFRTyr1068 protein levels normalized to GAPDH in n= 3 independent experiments. Significance was determined by two-way ANOVA followed by Šídák's multiple comparisons test. **E)** Cells were reverse transfected with 20nM siRNA: siCtrl (control) and two different siSNX10 oligoes (siSNX10#1 and siSNX10#2) prior to fixation and staining for

endogenous EEA1. Images were taken with Zeiss Axio Observer widefield microscope (Zen Blue 2.3, Zeiss) and a 20x objective was used. Scale bar: 10 µm. **F)** quantification of the data shown in E) was performed using CellProfiler software. The values were obtained from analyzing >1000 cells per condition and they were normalized to control siRNA (siCtrl). The graphs display the mean values ±SEM from n = 3 independent experiments. The significance was assessed by ordinary one-way ANOVA followed by Bonferroni's post hoc test. (* = $p < 0.05$). **G)** Representative electron microscopy images of U2OS cells (control and siSNX10) showing immunogold-labelled EGFR containing endosomes. One experiment was performed. The number of endosomes without EGFR-gold and with EGFR-gold of which diameter was measured were 8 (siCtrl), 45 (siSNX10), and 23 (siCtrl), 10 (siSNX10) respectively. **H)** The graph displays the mean values ± SEM from the endosomal diameters. Significance was determined by unpaired t-test with Welch's correction. * = $p < 0.05$, ** = $p < 0.01$, *** = $p < 0.001$, **** = $p < 0.0001$ and n.s = not significant in all graphs.

Figure 3. SNX10 interacts with mitochondria

A) U2OS cells expressing either WT SNX10-EGFP or the Y32S mutant underwent GFP pulldown for the subsequent analysis of their interactome using mass spectrometry assays. The resulting data were depicted in a Venn diagram, illustrating the distinct and shared interactors between the WT and mutant forms of SNX10. Significant identified proteins representing hits that interacted with SNX10 WT are listed below **B)** The interacting proteins of SNX10 WT were enriched for GO term analysis. The enrichment of the Cellular Component they belong to (pie chart above) and Biological Processes they are involved in (pie chart below) is expressed in percentage towards the significant hits. Graphs were plotted using plotly (python package). **C)** U2OS with stable inducible expression of SNX10-EGFP were treated with doxycycline for 24 hrs before incubation with MitoTracker Red for 30 min, followed by live imaging using a Dragonfly 505 (Andor) microscope, with an acquisition speed of 1 frame every 500 ms. Scale bar: 10 µm. **D)** U2OS cells stably expressing mScarlet-RAB5 and with inducible expression of SNX10-EGFP and were stained with MitoTracker Deep Red FM in the presence or absence of DFP. Scale bar 10 µm. **E)** U2OS SNX10-EGFP were treated with or without DFP (1 µM) for 24 hrs and with or without MRT68921 (1 µM) for 1 h. MitoTracker (100 nM) was added for 1 h, followed by immunofluorescence staining with antibodies against LC3B and COX-IV. Scale bars: 10 µm. **F and**

G) Quantification of the percentage of SNX10 localizing on LC3B (F) and LC3 + MitoTracker positive structures localizing on SNX10 (G), normalized to control sample (-MRT/-DFP) (the graph shows mean ± SEM [error bars] from n=3 independent experiments. The statistical significance was calculated with a two-way ANOVA followed by a Tukey's post analysis test. * = $p < 0.05$)

Figure 4. SNX10 regulates the degradation of mitochondrial proteins

A) U2OS cells with stable inducible expression of SNX10-EGFP were pre-treated with doxycycline for 16 hrs before the addition of DFP for 24 hrs. The cells were fixed and stained with antibodies against mitochondrial proteins for subsequent analysis. Scale bars: 10 µm. **B)** U2OS cells were reverse transfected with the indicated siRNA (20 nM) for 48 hrs, then treated or not with DFP for 24 hrs with BafA1 treatment or not the last 2 hrs, followed by western blotting for the indicated proteins. **C-E)** Quantification of the data in B) from n=5, 3 and 6 independent experiments. Bars show mean values of the protein levels normalized to b-Actin relative to Control conditions (siCtrl control). Significance is assessed by two-way ANOVA followed by Tukey's post hoc test. **F)** U2OS cells were subjected to reverse transfection with siSNX10 (20nM) for 48 hours, followed by treatment with either IN1 or MRT for 24 hours before fixation. Post-fixation, cells were stained with a COX-IV antibody, and images were captured using an ImageXpress Micro Confocal (Molecular Devices) at 20X magnification. * = $p < 0.05$, ** = $p < 0.01$, *** = $p < 0.001$, **** = $p < 0.0001$ and n.s = not significant in all graphs

Figure 5. SNX10 is important for mitochondrial bioenergetics

A) Citrate Synthase activity was determined by spectrophotometry from lysates of U2OS cells transfected with siRNA for 72 hrs, in the presence or absence of DFP for the last 24 hrs. The graph displays mean values normalized to siCtrl. Significance was determined from n = 3 independent experiments, by two-way ANOVA followed by Tukey's multiple comparison test. **B)** Mitochondrial oxygen consumption rate (OCR) was assessed in control and SNX10 knocked down cells using the Seahorse XFe24 Analyzer. OCR was measured following sequential addition of Oligomycin, carbonyl cyanide m-chlorophenyl hydrazone (CCCP), and Rotenone/Antimycin A (Rot/AntiA). **C)** The four basal OCR measurements per well were averaged to determine the basal OCR value, and non-mitochondrial respiration was subtracted to ascertain the basal respiration associated with each condition. **D)** ATP production was calculated by subtracting the proton leak from the maximal respiratory capacity. Error bars represent mean ± SEM from n=5. Statistical significance

was determined using one-way ANOVA followed by Dunnett's multiple comparison test. * = $p < 0.05$, ** = $p < 0.01$, *** = $p < 0.001$, **** = $p < 0.0001$ and n.s = not significant in all graphs

Figure 6. SNX10 regulates mitochondrial homeostasis and cell death in vivo

A) Overview and schematic diagram of human SNX10, zebrafish Snx10a and Snx10b proteins. Percentage identity of PX domain on comparison with human counterpart shown below the zebrafish PX domains. Also shown is the percentage identity of the orthologues amongst each other. **B)** Temporal expression pattern of *snx10a* and *snx10b*. The graph shows the fold change in transcript levels relative to β-actin in whole zebrafish embryos from 1 dpf to 5 dpf. Error bars indicate mean ± SEM. Data is collected from 3 individual experiments. **C)** Dorsal and lateral view of spatial expression pattern of *snx10a* and *snx10b* at 3 dpf as demonstrated by whole-mount in situ hybridization (WM-ISH) using an internal (INT) probe. Scale bar = 200 µm. Images are representative from 3 experiments. **D)** Representative immunoblots of Snx10 and β-tubulin on whole embryo lysates from control (scrambled guide) and single or double *snx10a/snx10b* KO (DKO) animals. β-tubulin served as loading control. **E)** Representative immunoblots of Snx10, Samm50, Cox4 and Actin on whole embryo lysates from control (scrambled guide) and *snx10ab* DKO. **F)** Quantification of the Cox4 signal intensities from blots in (Fig 7E) normalized to control_DMSO signal intensity. Error bars indicate mean ± SEM. *$p < 0.05$, **$p < 0.005$, ***$p < 0.0005$, unpaired Students t-test. Experiment was performed 4 times. **G)** Quantification of the Samm50 signal intensities from blots in (Fig 5E) normalized to control_DMSO signal intensity. Error bars indicate mean ± SEM. *$p < 0.05$, **$p < 0.005$, ***$p < 0.0005$, unpaired Students t-test. **H)** Representative images of TUNEL assay on control (scrambled sgRNA) and *snx10ab*_DKO larvae treated with or without 100um DMOG at 3 dpf. Orientation lateral. Scale bar is 200 µm. **I)** Quantification of mean fluorescent intensity from demarcated brain region of images in (H). A total of 45 control larvae (scrambled sgRNA) treated with or without DMOG and 41 *snx10ab*_DKO larvae with no DMOG treatment were used for quantification, respectively. Values were normalized to control_DMSO values. Experiment was performed 2 times. Plots demonstrate data distribution and median value (red line). Significance was determined by two-way ANOVA followed by Tukey's post-test to compare all groups. **J)** Quantification of ROS levels obtained via FACS analysis of control (scrambled sgRNA), *snx10ab*_DKO and positive control larvae at 3 dpf incubated with MitoSOX. The values presented as relative values after normalizing to control.

Quantification was from at least 2 independent experiments. Error bars indicate mean ± SEM. *$p < 0.05$, **$p < 0.005$, ***$p < 0.0005$, unpaired Students t-test with Welch's correlation.

Figure 1

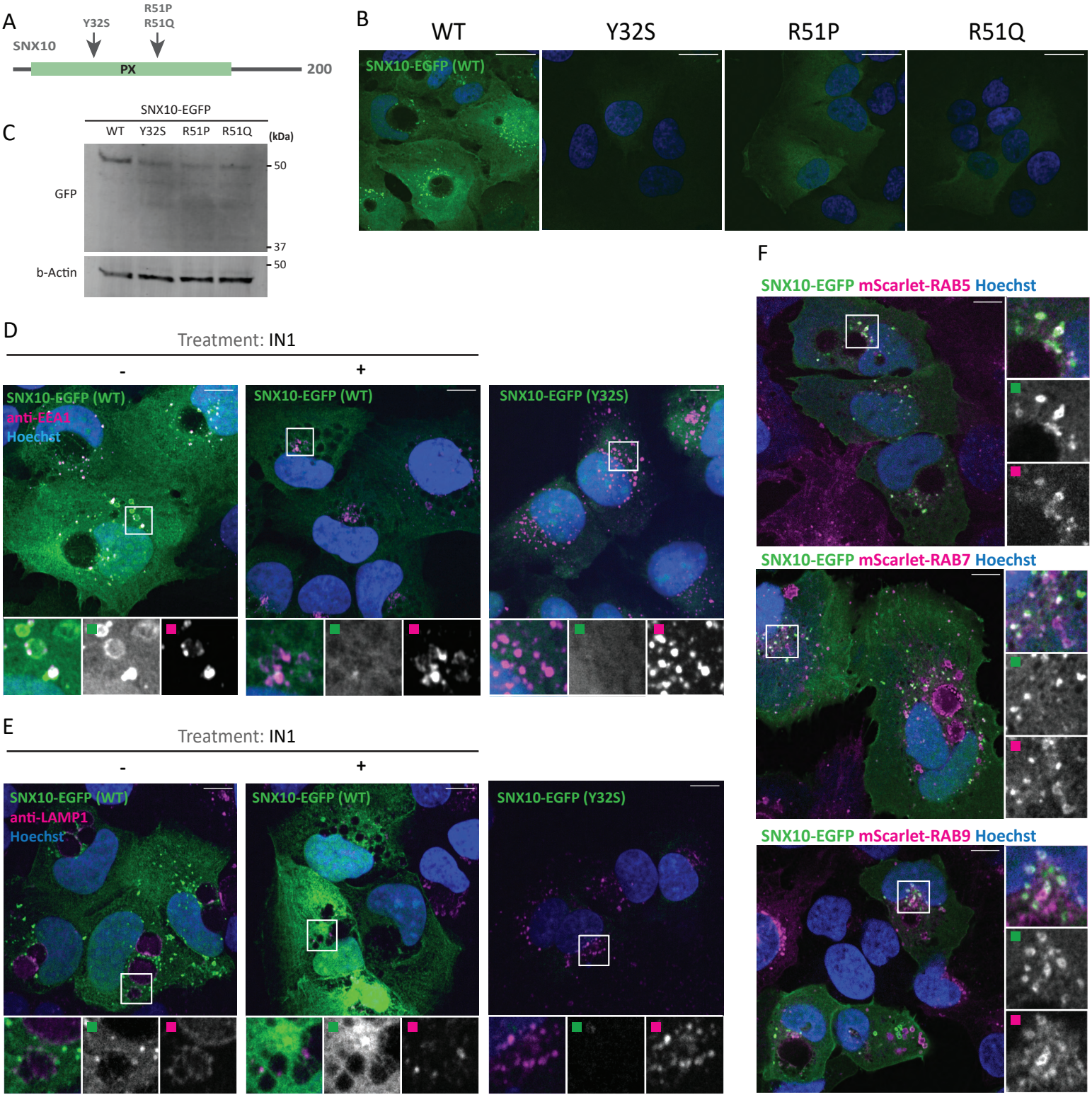
A
SNX10
Y32S
R51P
R51Q
PX
200
B
WT
Y32S
R51P
R51Q
SNX10-EGFP (WT)
C
SNX10-EGFP
WT
Y32S
R51P
R51Q
(kDa)
GFP
b-Actin
50
37
50
D
Treatment: IN1
-
+
SNX10-EGFP (WT)
anti-EEA1
Hoechst
SNX10-EGFP (WT)
SNX10-EGFP (Y32S)
E
Treatment: IN1
-
+
SNX10-EGFP (WT)
anti-LAMP1
Hoechst
SNX10-EGFP (WT)
SNX10-EGFP (Y32S)
F
SNX10-EGFP mScarlet-RAB5 Hoechst
SNX10-EGFP mScarlet-RAB7 Hoechst
SNX10-EGFP mScarlet-RAB9 Hoechst

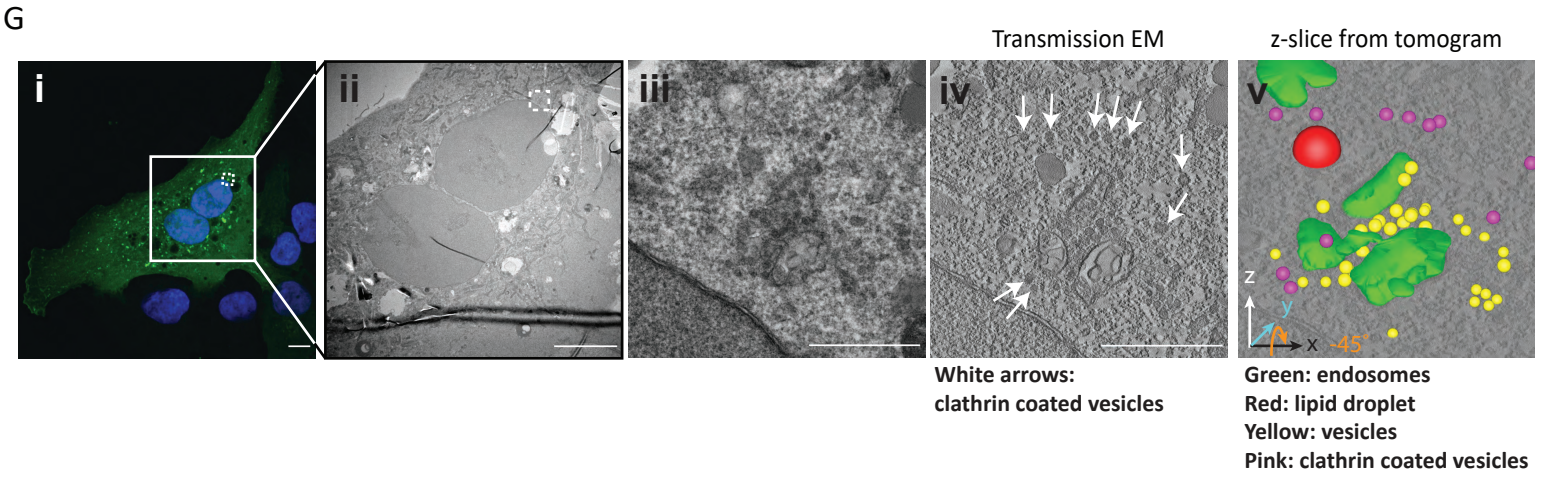
G
i
ii
iii
Transmission EM
iv
z-slice from tomogram
v
z
y
x
-45°
White arrows:
clathrin coated vesicles
Green: endosomes
Red: lipid droplet
Yellow: vesicles
Pink: clathrin coated vesicles

Figure 2

A

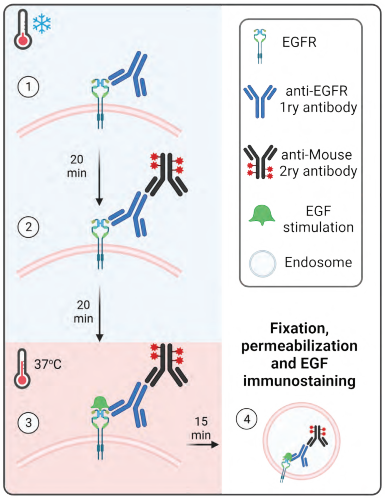

B

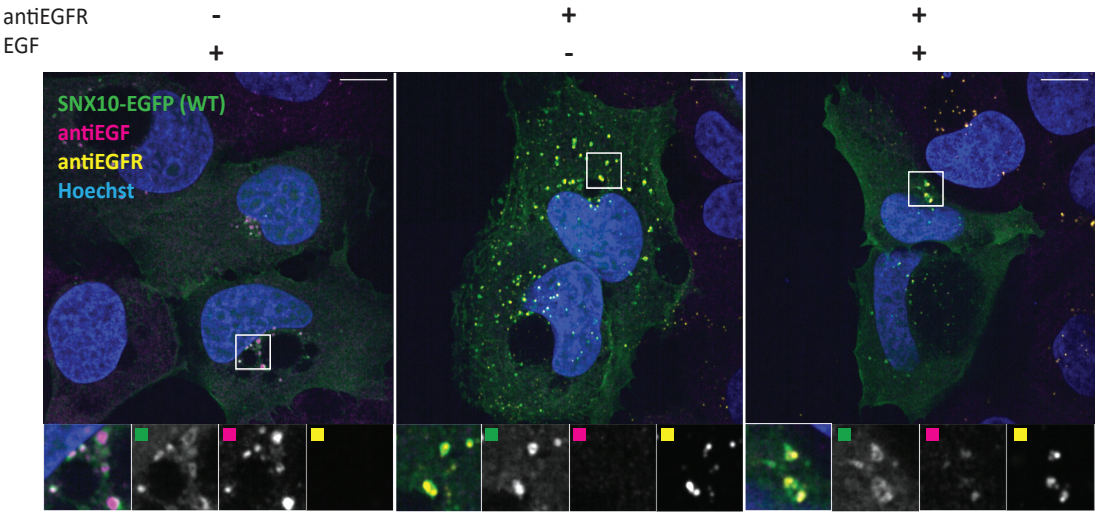

C

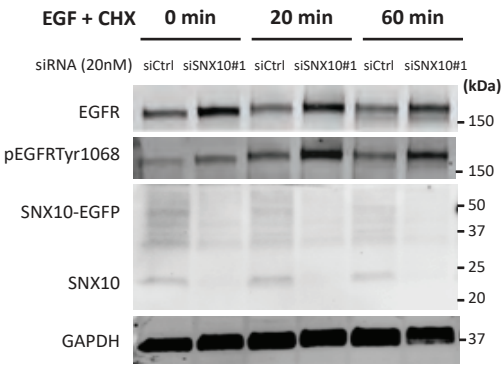

D

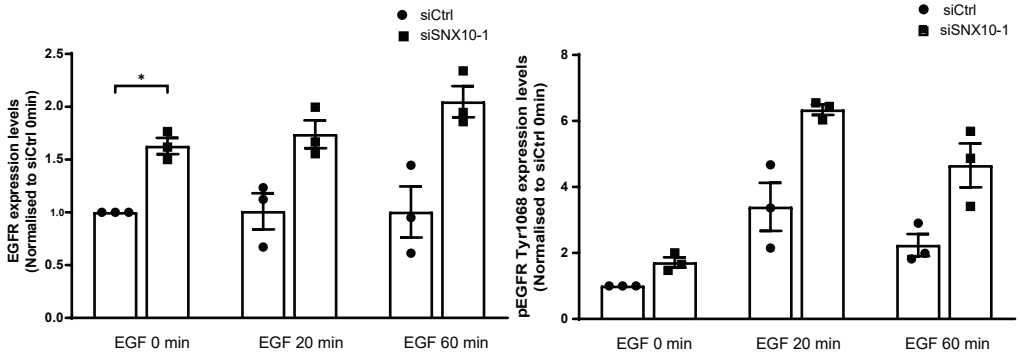

E

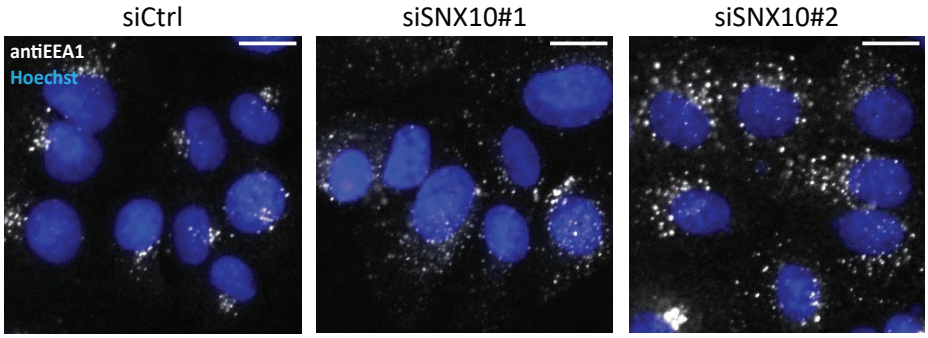

F

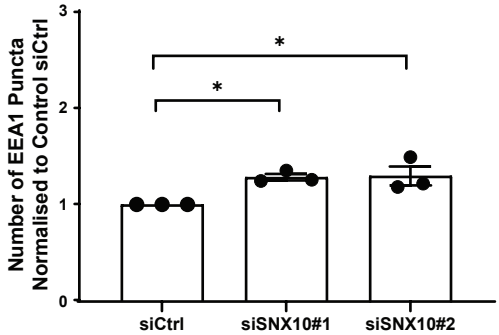

G

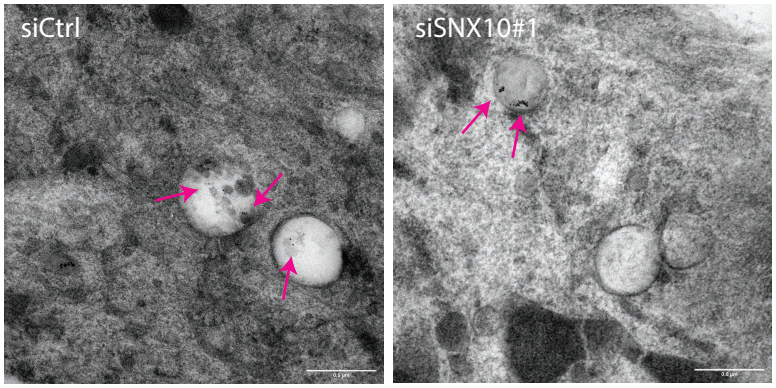

H

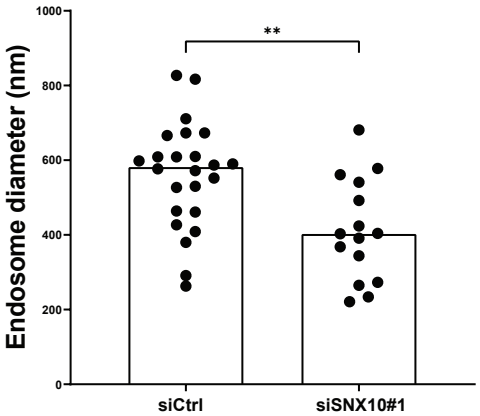

Figure 3

A

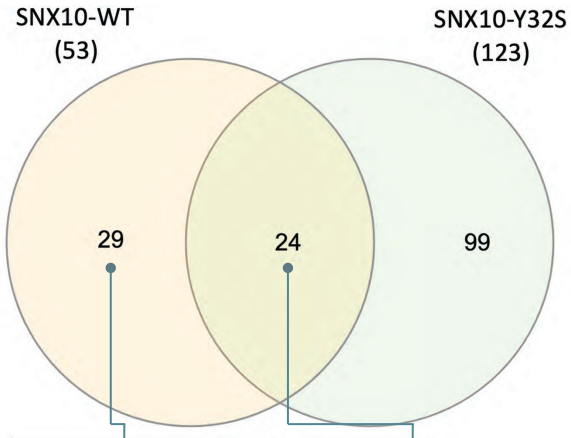

ATP5J	GNAO1	SEC24B
ATPIF1	IGHV3-38	SERPINH1
C10orf35	LAMTOR1	SPCS2
CTBP2	MVB12A	SPTLC2
DLST	NUBP1	SUCLG1
EEF1B2	PTGES2	TMA7
EEF1G	RBBP4	U2AF1
EIF3C	RBM22	UQCRFS1
EPB41L3	RCN1	VARS
GBA	RPL9	

ACTA1	MRPS36	TMEM109
CAPRIN1	RPL37A	YBX1
CAPZA2	RPS29	YBX3
CCDC47	SET	YWHAG
COX-IV	SFPQ	
EIF4B	SLC25A6	
EZR	SNX10	
GOSR1	SQSTM1	
HNRNPDL	TECR	
HSPA1A	TIGAR	

B

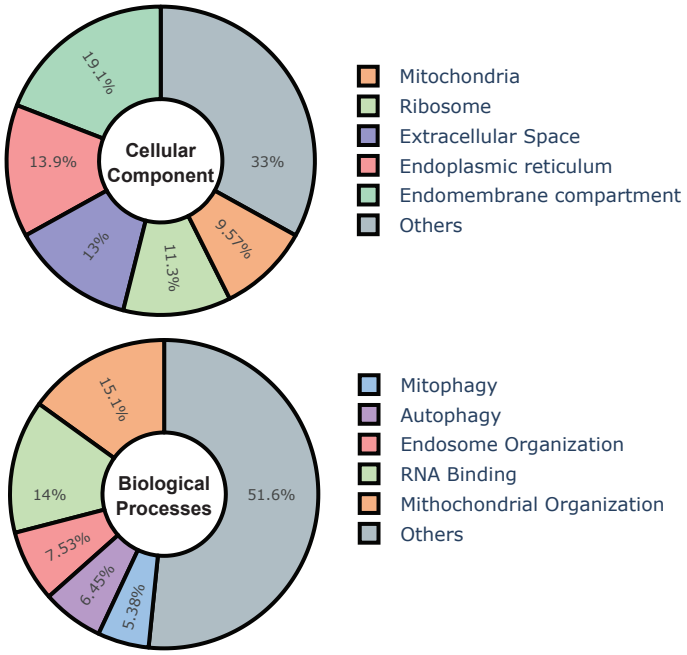

C

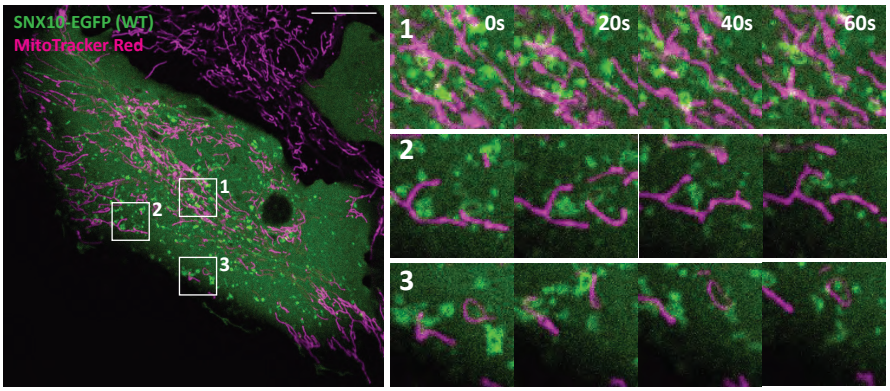

D

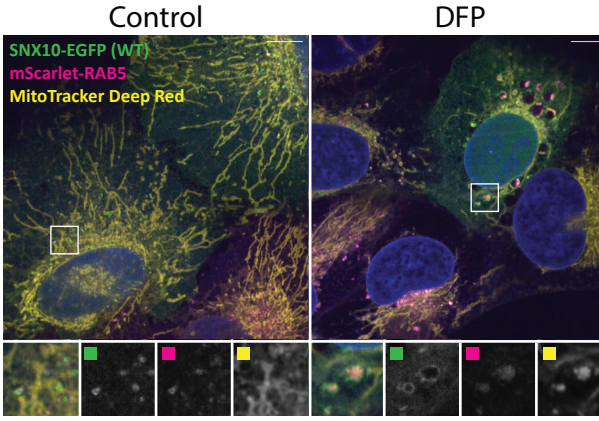

E

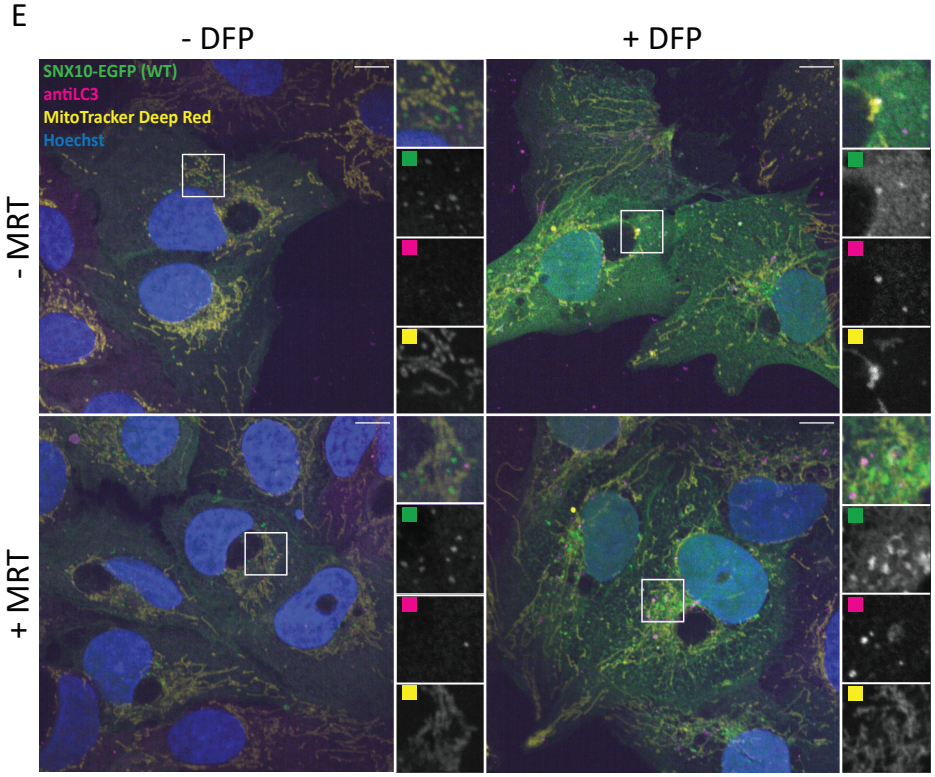

F

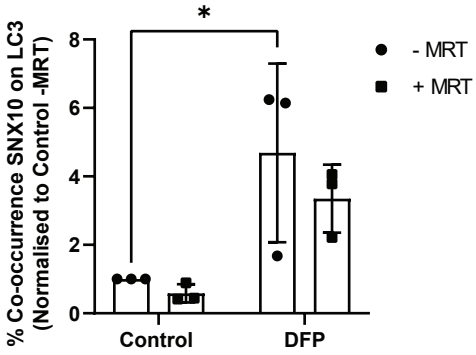

G

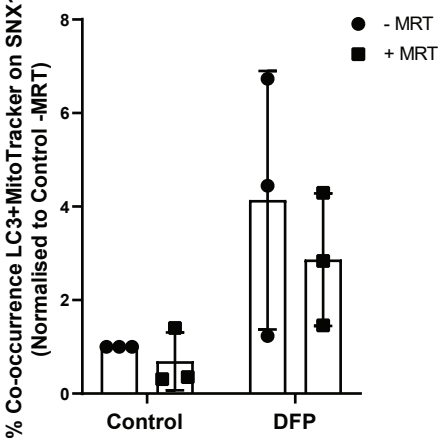

Figure 4

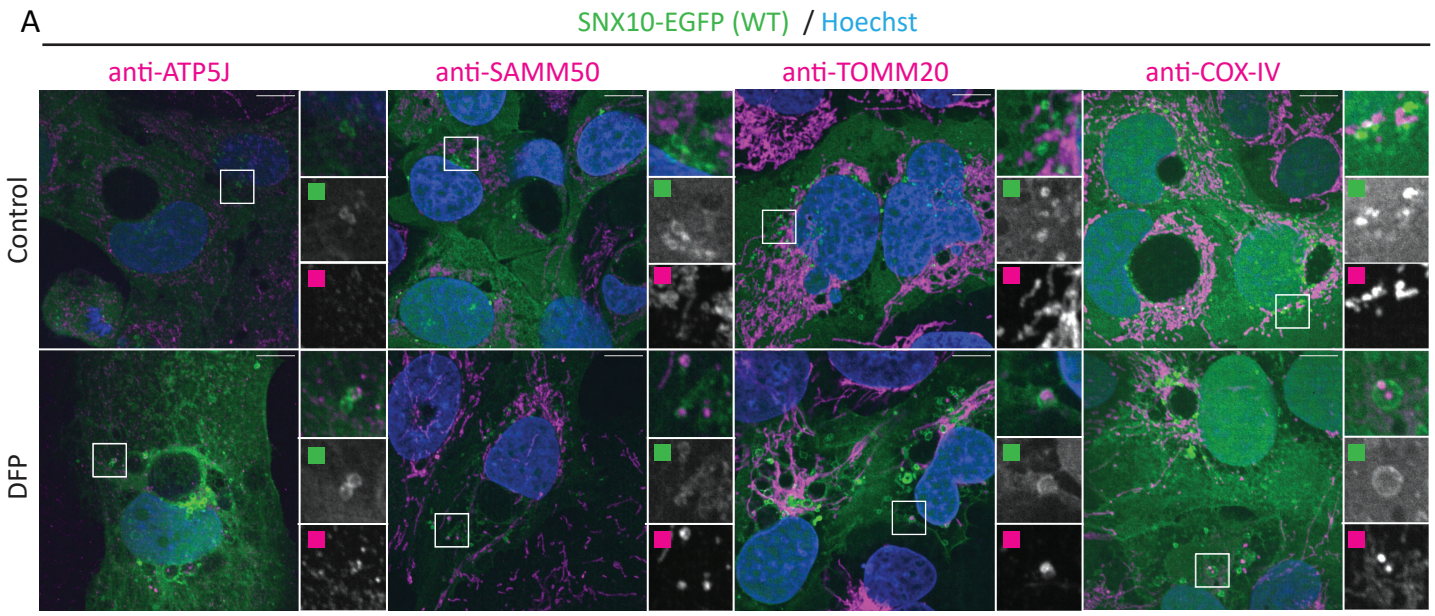
A
SNX10-EGFP (WT) / Hoechst
anti-ATP5J
anti-SAMM50
anti-TOMM20
anti-COX-IV
Control
DFP

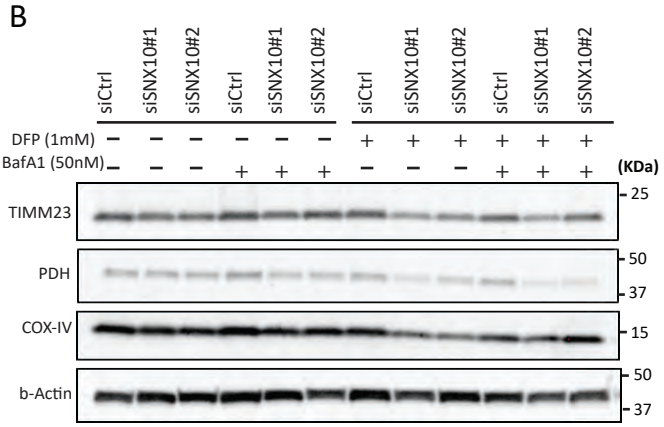
B
siCtrl
siSNX10#1
siSNX10#2
DFP (1mM)
BafA1 (50nM)
(KDa)
TIMM23
PDH
COX-IV
b-Actin
25
50
37
15
50
37

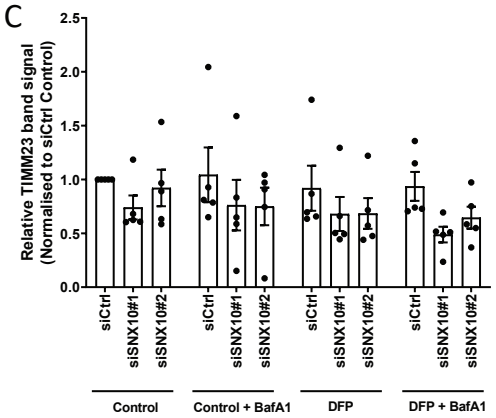
C
Relative TIMM23 band signal
(Normalised to siCtrl Control)
Control
Control + BafA1
DFP
DFP + BafA1

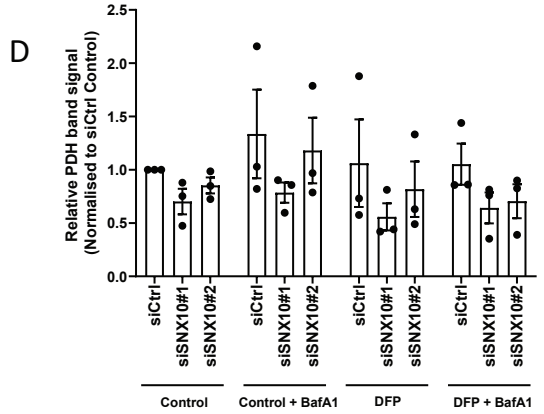
D
Relative PDH band signal
(Normalised to siCtrl Control)
Control
Control + BafA1
DFP
DFP + BafA1

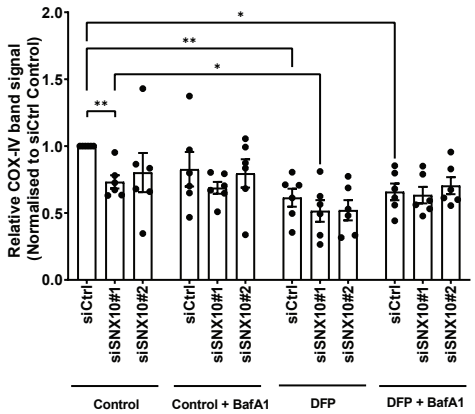
E
Relative COX-IV band signal
(Normalised to siCtrl Control)
Control
Control + BafA1
DFP
DFP + BafA1

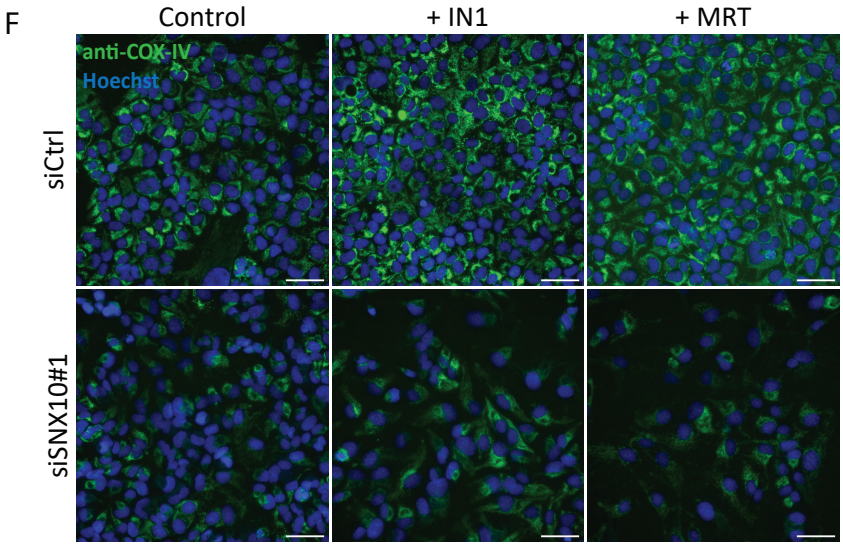
F
Control
+ IN1
+ MRT
anti-COX-IV
Hoechst
siCtrl
siSNX10#1

Figure 5

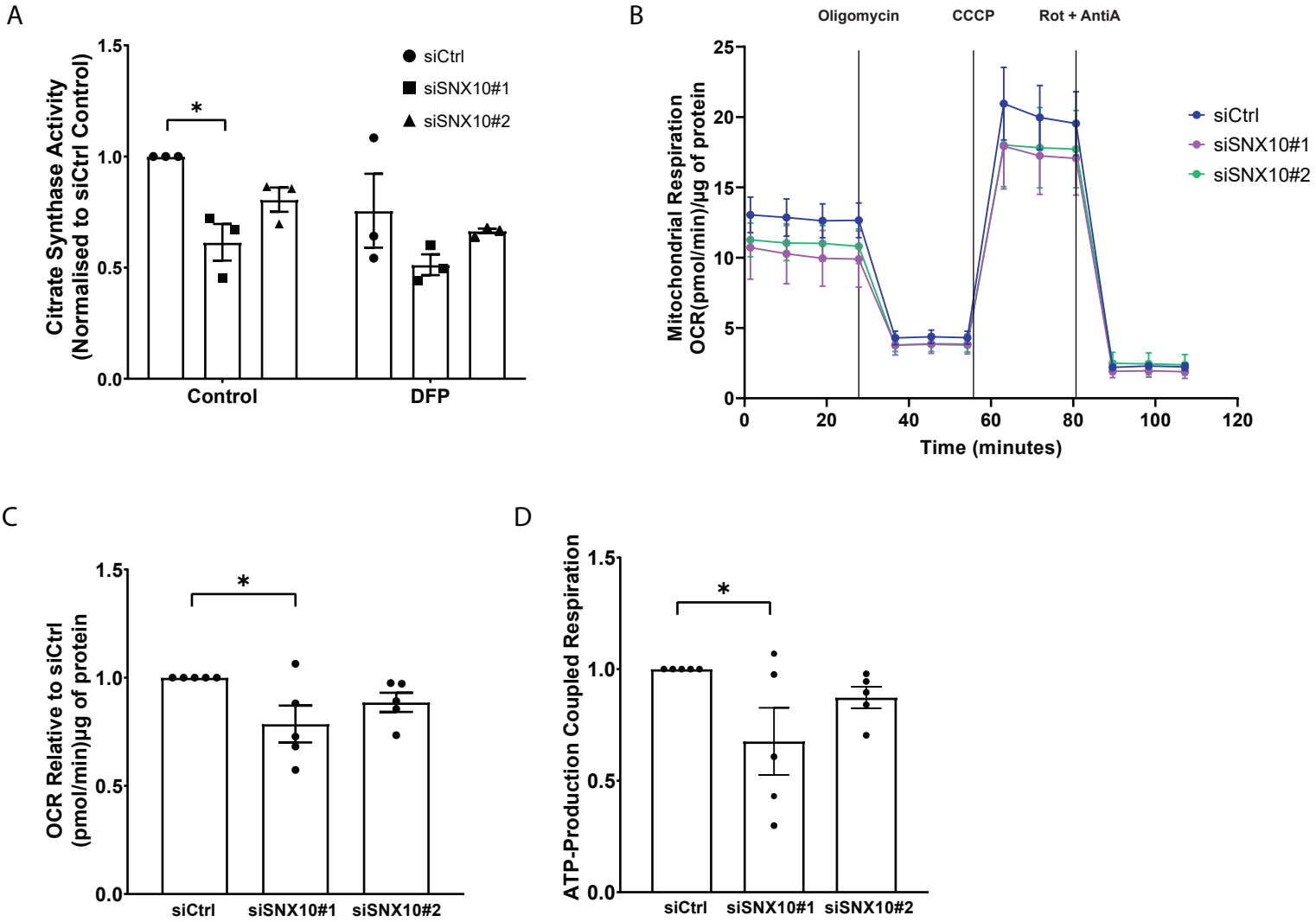
A
Citrate Synthase Activity
(Normalised to siCtrl Control)
1.5
1.0
0.5
0.0
*
siCtrl
siSNX10#1
siSNX10#2
Control
DFP
B
Oligomycin
CCCP
Rot + AntiA
Mitochondrial Respiration
OCR(pmol/min)/µg of protein
25
20
15
10
5
0
0
20
40
60
80
100
120
Time (minutes)
siCtrl
siSNX10#1
siSNX10#2
C
OCR Relative to siCtrl
(pmol/min)µg of protein
1.5
1.0
0.5
0.0
*
siCtrl
siSNX10#1
siSNX10#2
D
ATP-Production Coupled Respiration
1.5
1.0
0.5
0.0
*
siCtrl
siSNX10#1
siSNX10#2

Figure 6

A

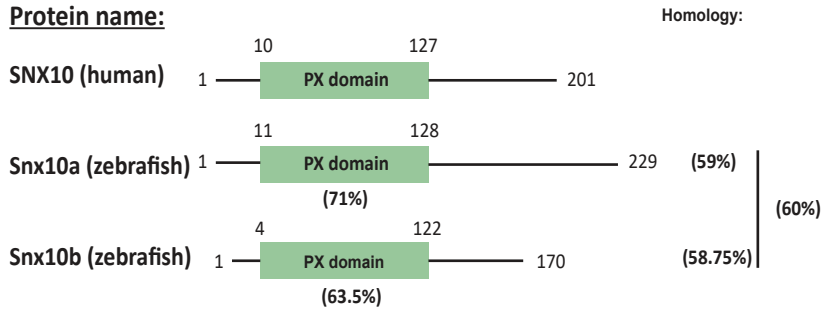

B

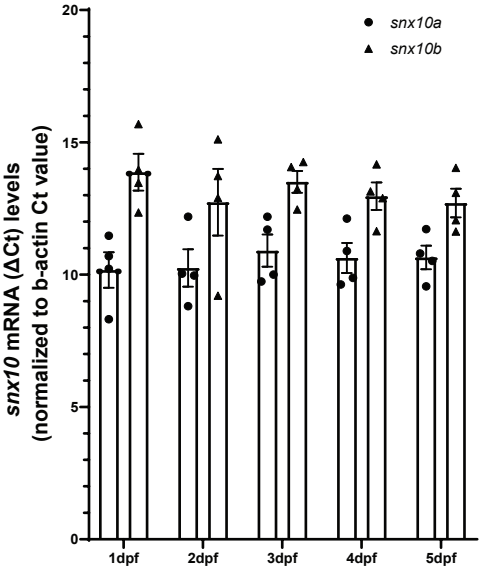

C

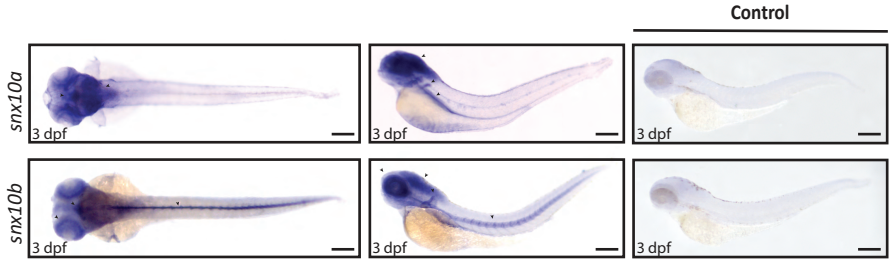

D

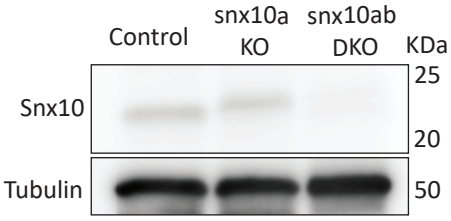

E

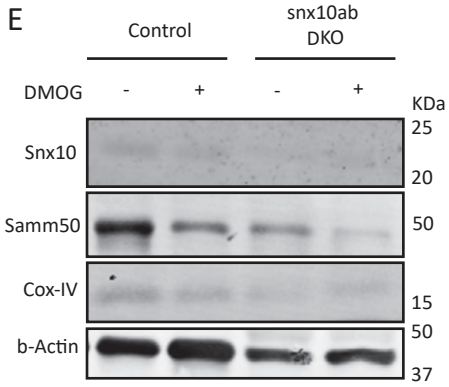

F

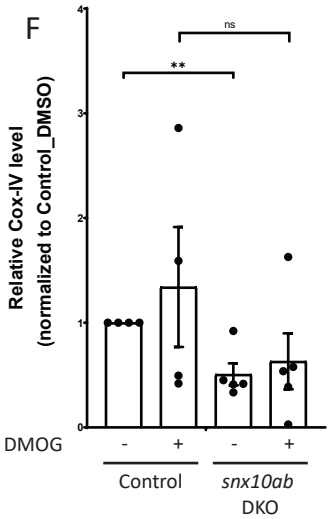

G

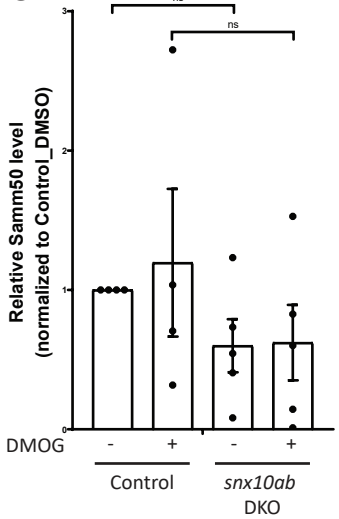

H

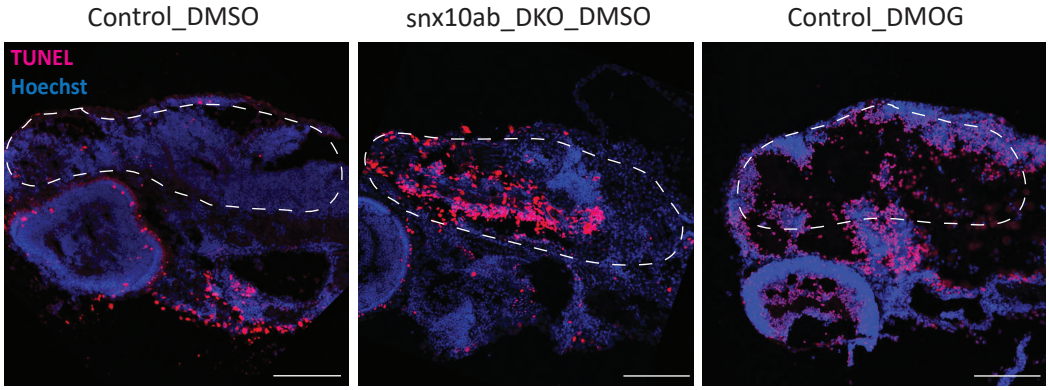

I

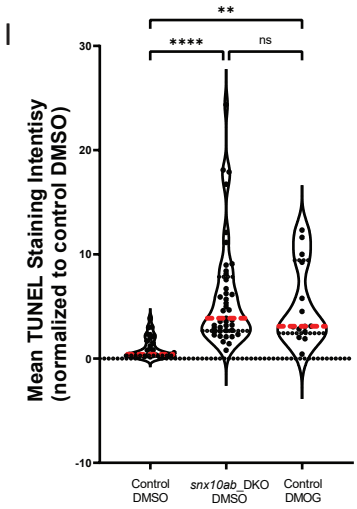
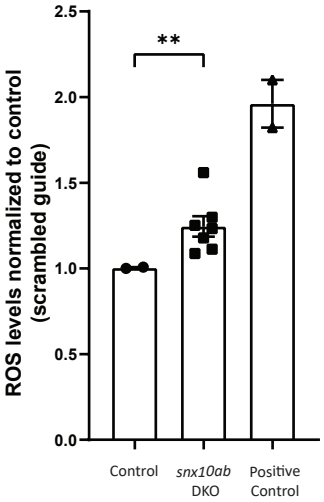
J